AIAA JOURNAL
Vol. 47, No. 11, November 2009

Bifurcation Behavior of Airfoil Undergoing Stall Flutter Oscillations in Low-Speed Wind Tunnel

Grigorios Dimitriadis*
Université de Liège, 4000 Liège, Belgium
and
Jing Li†
University of Manchester, Manchester, England M60 1QD, United Kingdom

DOI: 10.2514/1.39571

Stall flutter is a nonlinear aeroelastic phenomenon that can affect several types of aeroelastic systems such as helicopter rotor blades, wind turbine blades, and highly flexible wings. Although the related aerodynamic phenomenon of dynamic stall has been the subject of many experimental studies, stall flutter itself has rarely been investigated. This paper presents a set of experiments conducted on a NACA0012 airfoil undergoing stall flutter oscillations in a low-speed wind tunnel. The aeroelastic responses are analyzed with the objective of characterizing the local bifurcation behavior of the system. It is shown that symmetric stall flutter oscillations are encountered as a result of a subcritical Hopf bifurcation, followed by a fold bifurcation. The cause of these bifurcations is the occurrence of dynamic stall, which allows the transfer of energy from the freestream to the wing. A second bifurcation occurs at the system's static divergence airspeed. As a consequence, the wing starts to undergo asymmetric stall flutter bifurcations at only positive (or only negative) pitch angles. The dynamic stall mechanism itself does not change but the flow only separates on one side of the wing.

I. Introduction

THE subject of this paper is the experimental study of the aeroelastic behavior of a wing undergoing stall flutter. A series of experiments carried out on a wing with pitch and plunge degrees of freedom in a low-speed wind tunnel are described and the results are analyzed to attempt a characterization of the stall flutter phenomenon.

Classical bending-torsion flutter involves the interaction between two or more modes of vibration (or degrees of freedom) to give rise to catastrophic self-excited vibrations of exponentially increasing amplitude. The phenomenon is treated using linear assumptions, and methods for its prediction are at a quite advanced stage.

Stall flutter is a nonlinear dynamic phenomenon that can involve only a single degree of freedom. It is associated with large areas of dynamically separating and reattaching flow over a lifting surface. Stall flutter is closely related to galloping; in fact, Blevins [1] treats the two phenomena simultaneously because they are both oscillations of limited amplitude, induced by unsteady separated flows. Stall flutter involves stalled flow over wings, whereas galloping involves separated flow over bluff bodies. The main difference between the two is that, in stall flutter, the flow reattaches instantaneously during an oscillation cycle, whereas flow over bluff bodies is always separated. In this paper, only stall flutter will be considered, that is, the work will concern a wing.

Essential to the occurrence of stall flutter is the phenomenon of dynamic stall, even though these two are quite distinct phenomena. As this distinction is central to the present work, the definitions of the two phenomena is given here.

Dynamic stall: The significant and abrupt loss of aerodynamic loads (lift and/or pitching moment) due to flow separation on wings undergoing unsteady motions. It is an unsteady aerodynamic phenomenon.

Stall flutter: Self-excited oscillation of limited amplitude, caused by the interaction of a dynamic stall event with the inertial and elastic characteristics of a wing. It is an aeroelastic phenomenon.

Dynamic stall is a purely aerodynamic phenomenon because no feedback from the aerodynamic forces to the motion of the wing is necessary for it to occur. In dynamic stall experiments, the motion of the wing is prescribed using motors and the wing itself is usually completely rigid. Stall flutter, on the other hand, is an aeroelastic phenomenon because the dynamically stalling aerodynamic forces interact with the structural restoring forces of the wing and the motion is a free self-excited oscillation of limited amplitude. In the nonlinear dynamics literature, such oscillations are called limit cycle oscillations (LCOs). In other words, dynamic stall is an aerodynamic nonlinearity. Stall flutter is a LCO occurring as a result of the existence of this nonlinearity.

Nevertheless, dynamic stall is the phenomenon that has been most investigated in the past. Halfman et al. [2] produced one of the first truly thorough investigations of dynamic stall. Experimental results in a wind tunnel were obtained using an airfoil oscillator, that is, a mechanism for forcing a nearly 2-D rectangular NACA wing to oscillate sinusoidally in a wind-tunnel section. Time-varying lift, drag, moment, and position were measured along with various inertia quantities.

Ericsson and Reding [3–5] carried out a significant amount of work on dynamic stall in the 1970s. Among other things, they developed a quasi-steady aerodynamic model for dynamic stall of a 2-D airfoil with unsteady terms represented by a single lumped vortex "spilled" from the trailing edge. The authors' quasi-steady approach was further improved by including in the analysis the effect of this spilled leading-edge vortex [6].

McCroskey [7] defined two dynamic stall regimes: light stall and deep stall. Light stall is a phenomenon similar to static stall and is characterized by very negative pitch damping values. Deep stall is essentially the phenomenon whereby a large vortex is shed at the leading edge and travels downstream. The passage of this vortex over the airfoil's upper surface produces maximum lift and moment values far in excess of their static counterparts.

Several other experimental investigations of dynamic stall were carried out since then, including particle image velocimetry measurements [8,9], culminating in a nearly complete visualization of the dynamic stall phenomenon [10].

Received 4 July 2008; revision received 26 May 2009; accepted for publication 5 July 2009.

*Assistant Professor, Département d'Aérospatiale et Mécanique, B52/3, Chemin des Chevreuils, 1; gdimitriadis@ulg.ac.be. Member AIAA.

†Researcher, Post Office Box 88.

On the other hand, research on stall flutter itself has been quite rare. Early investigations [11,12] stated that the flexure-torsion flutter speed of wings decreases at high incidences. It was concluded that this decrease may be due to a reduction of aerodynamic torsional damping with incidence.

In the 1960s, Ham and Young [13] defined stall flutter as an oscillation of a wing (or helicopter blade) during which the time-averaged damping in pitch is exactly zero over a cycle of the oscillation. Such oscillations are self-excited and self-limiting, that is, limit cycle oscillations.

In the early 1990s, the Structural Dynamics Division at NASA Langley Research Center initiated the Benchmark Models Program. Results from wind-tunnel flutter tests on a 3-D wing with a NACA0012 section [14] showed that stall flutter can occur at some combinations of dynamic pressure and angle of attack. The full flutter boundary was traced, including the stall flutter boundary.

It could be argued that the conceptually difficult aspect of the stall flutter phenomenon is the aerodynamic side; the structural behavior is linear and therefore easy to describe. However, in these authors' opinion the separation of the aerodynamic and structural aspects of stall flutter and the study of only the aerodynamic side to characterize the full phenomenon is incomplete. Stall flutter is a nonlinear phenomenon. Even if the nonlinearity comes uniquely from the aerodynamic forces, the principle of superposition does not hold. In other words, a nonlinear dynamic system cannot always be conveniently split into linear and nonlinear subsystems. Changes in the linear subsystem can completely change the character of the response of the complete system.

The purpose of the present work is to investigate the complete aeroelastic phenomenon of stall flutter. Experiments will be described concerning the stall flutter behavior of a NACA0012 airfoil and the parameters that influence this behavior will be explored. The airfoil has pitch and plunge degrees of freedom, restrained by torsional and compression springs, respectively. The pitch and plunge displacements, as well as the pressure distribution around the midspan section, are measured. The nonlinear dynamic response will be characterized in terms of local bifurcations and the changes in bifurcations with some of the controlling parameters will be investigated.

First, the experimental setup will be described, followed by the presentation of static aerodynamic measurements on the wing. Then, the wing's dynamic responses will be presented and analyzed and the occurrence of stall flutter oscillations highlighted. Finally, the complete stall flutter behavior of the wing in the speed range tested will be detailed, bifurcation analysis will be carried out, and physical justifications will be attempted for the various phenomena observed.

II. Experimental Setup

The experiments were carried out in the Goldstein Laboratory of the University of Manchester. Two different wind tunnels were used. The static tests were performed in the Project tunnel, and the dynamic tests presented in this paper were conducted in the Avro 9×7 ft tunnel. The Project tunnel is an open-return subsonic wind tunnel. Its working section is 2.16 m in length, 1.1 m in width, and 0.86 m in height. The cross-sectional area is 0.782 m^2, forming an octagonal shape with four 45 deg corner fillets. The fan can provide a flow velocity in the working section from 5 to 55 m/s. The Avro 9×7 ft tunnel is a closed-return subsonic wind tunnel, with a test section 2.74 m wide, 2.1 m high, and 5.5 m long ($9 \times 7 \times 18$ ft) and a contraction ratio of 6:1. The maximum speed is 70 m/s.

The experimental apparatus consisted of a wing model, the support mechanism, the sensors, data recording equipment, and either of the two wind tunnels. The wing chosen for this experiment is a rectangular wing with NACA0012 airfoil section, with 900 mm span, 300 mm chord, and an aspect ratio $AR = 3$. This airfoil was chosen because it is most often used for theoretical and experimental research programs. The wing was fitted with clear end plates to constrain the flow to be quasi-two-dimensional. The internal structure of the wing consisted of four aluminum ribs with NACA0012 shape. The ribs were secured on a square shaft, positioned 0.115 m behind the leading edge. This shaft acted as the pitch axis, that is, the wing could pitch around it.

The support mechanism was designed to allow pitch and plunge motion of the wing model without friction and with known structural stiffness. Restoring force was provided by two pairs of compression springs and a pair of torsion springs. One or both degrees of freedom could be locked down. As shown in Fig. 1, the model was tailored to fit in both tunnels. In the Project tunnel, the support structure was fixed on a steel platform placed under the tunnel; apart from the wing and end plates, all the components were placed outside the tunnel. In the 9×7 ft tunnel, the support mechanism was standing on two steel plates that were fixed on the tunnel floor by two steel bars. The wing assembly was mounted inside the tunnel. The attachment platforms used in both tunnels were not completely rigid, but their natural frequencies were much higher than the oscillation frequencies of the wing model and could be filtered out.

The motion of the wing was measured and recorded by means of two long-range laser displacement sensors. As shown in Fig. 1b, the sensors were fitted above the wing, illuminating a spot near the leading edge and one near the trailing edge. The two spots lay on the midspan line. From these measurements, the pitch and plunge displacements of the wing could be reconstructed. The pitch and plunge velocities were obtained by numerically differentiating the displacements. The motion of the wing was also recorded using a digital camera.

The pressure distribution around the midspan section of the wing was measured by means of 18 pressure transducers fitted inside the wing. The piezoresistive pressure sensors were specifically developed for this project to conform to the relatively low pressure variations and low frequencies characteristic of stall flutter [15].

The pressure transducers were mounted inside the wing and connected with short plastic tubes (about 20 mm in length) to pressure tappings on the surface of the skin. The pressure tappings were drilled on the wing's surface at the midspan section (nine on the upper and nine on the lower surface), at the positions shown in Fig. 2. They were located symmetrically on the upper and lower surfaces of the wing.

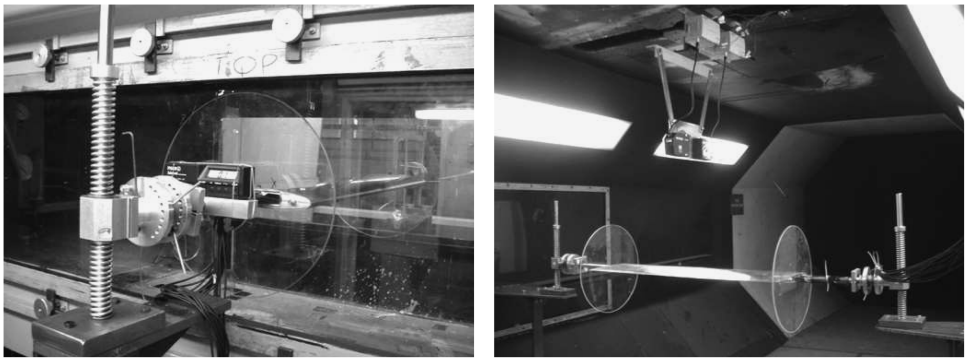

a) Wing in Project tunnel **b) Wing in 9×7 ft tunnel**

Fig. 1 Stall flutter wing shown in both tunnels.

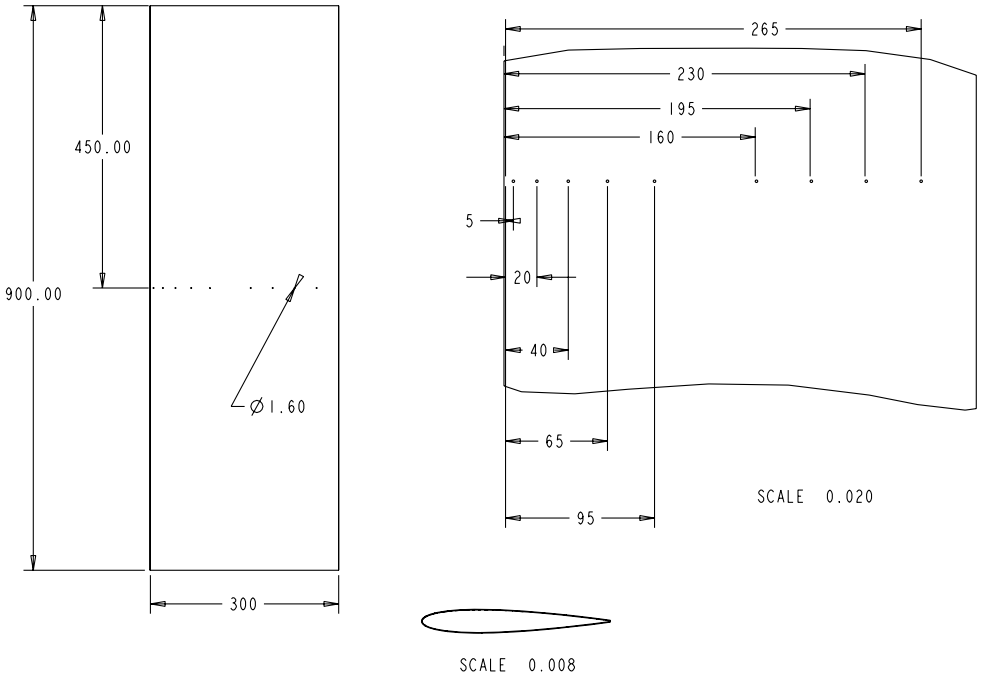

Fig. 2 Position of pressure tappings on the wing's surface.

The maximum test airspeed was limited to 30 m/s to ensure the structural integrity of the wing and its support structure. The minimum airspeeds tested were around 3 m/s; therefore, the Reynolds number range of the experiments extended from 6×10^4 to 6×10^5. Table 1 shows a summary of all the important experimental parameters.

III. Static Test Results

The static tests were performed to verify that the pressure transducers were accurate and also to quantify the static lift curve of the stall flutter wing and its dependence on Reynolds number. These tests consisted of clamping the wing at a particular pitch angle and measuring the pressure distribution around it for several airspeeds. The pressure distribution was integrated to calculate the aerodynamic lift and moment around the leading edge at various angles of attack and airspeeds.

Figure 3 shows the measured lift coefficient and pitching moment coefficient around the quarter-chord for angles of attack between -40 and $+40$ deg and airspeeds of 10, 15, 20, and 25 m/s. Here, lift is taken to mean the aerodynamic force in the vertical direction, not the force normal to the wing's chord. The corresponding Reynolds numbers were 2×10^4, 3×10^4, 4×10^4, and 5×10^4. Corrections for wind-tunnel effects were applied to the measured aerodynamic loads. It can be seen that there are small variations of the lift and moment coefficient curves with airspeed. The maximum lift coefficient is just under one at 10 m/s but increases to almost 1.2 at 25 m/s. At negative angles of attack, the lift coefficient reaches -1.1 at 25 m/s. The variation of the pitching moment coefficient curve with airspeed is less clear-cut but there is one obvious effect: at small angles of attack, the pitching moment coefficient is constant but not equal to zero. For a perfectly symmetric airfoil, the pitching moment coefficient around the quarter-chord should be zero when the flow is attached.

Table 1 Important experiment parameters

Experimental parameter	Value	Experimental parameter	Value
Wing span	0.9 m	Wing chord	0.3 m
Pitch axis position	0.115 m	Airspeed	0–30 m/s
Weight of wing assembly	15 kg	Moment of inertia around pitch axis	0.31 kgm^2
Stiffness in plunge	30.5 N/mm	Stiffness in pitch	13.1 Nm/rad

Both the lift and pitching moment coefficient curves show that the stall flutter wing is not perfectly symmetrical. The zero lift angle of attack lies between 1 and 2 deg, the positive stall angle is 13 deg, and the negative stall angle is 10 deg, and the pitching moment around the quarter-chord is small but nonzero at small angles of attack. There is clearly a small asymmetry in the wing, which will play a role in its stall flutter behavior, to be detailed in the next section. It should be noted, though, that the static stall angles do not change with Reynolds number.

The pitching moment coefficient around the quarter-chord was plotted in Fig. 3b for compatibility with the NACA airfoil measurements. However, for the dynamic tests, the pitching moment coefficient around the pitch axis was used. From now on, every mention of pitching moment will refer to the pitching moment around the pitch axis.

IV. Dynamic Test Results

The dynamic test procedure involved the setting of the desired wind-tunnel airspeed, the start of the measurement, and the subsequent excitation of the wing to measure its responses. The excitation was a large hand-administered impulsion, intended to drive the wing into angles of pitch high enough to stall the flow. The measurement of the position and pressure responses was always triggered simultaneously.

Figure 4 shows the position and aerodynamic load responses at an airspeed of 2.5 m/s. An impulse was applied to the wing, causing a response in both pitch and plunge, as seen in Fig. 4a. There is a significant pitch displacement of the order of 40 deg and a plunge displacement on the order of 8 cm. The aerodynamic loads responses (i.e., lift and moment around the pitch axis) are shown in Fig. 4b. The lift is defined as positive upward and the moment as positive nose up. It can be seen that they are very low, as expected because the airspeed is also low. The loads are presented as values per meter. Considering that the span is 0.9 m, the maximum instantaneous lift is about 2 N and the maximum instantaneous pitching moment is about 0.3 Nm. The response is highly damped and the motion stops after 2 cycles.

The result presented in Fig. 4 does not show any clear evidence of stall. The maximum values for the lift and moment occur at

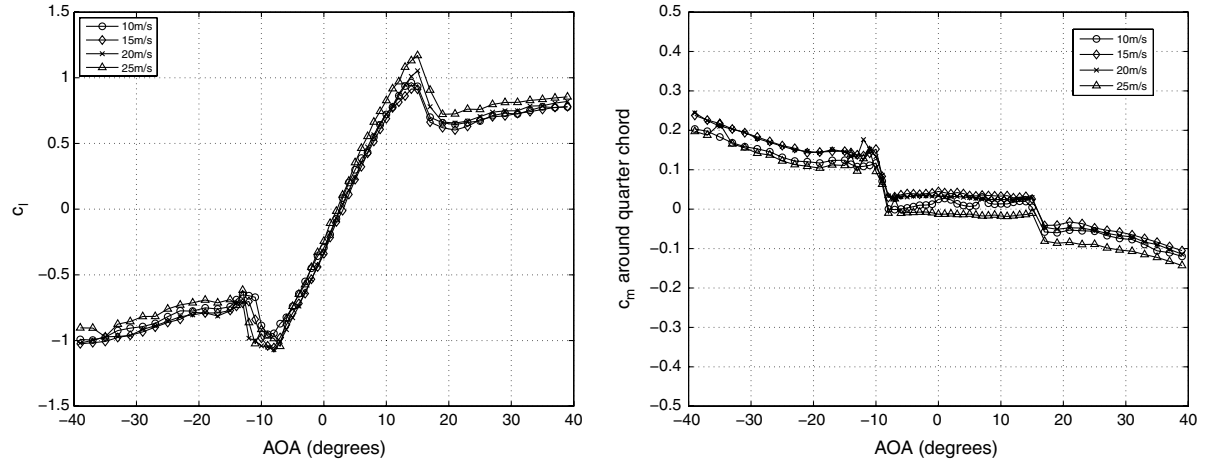

a) Lift coefficient

b) Pitching moment coefficient around quarterchord

Fig. 3 Static lift and pitching moment coefficient measurements.

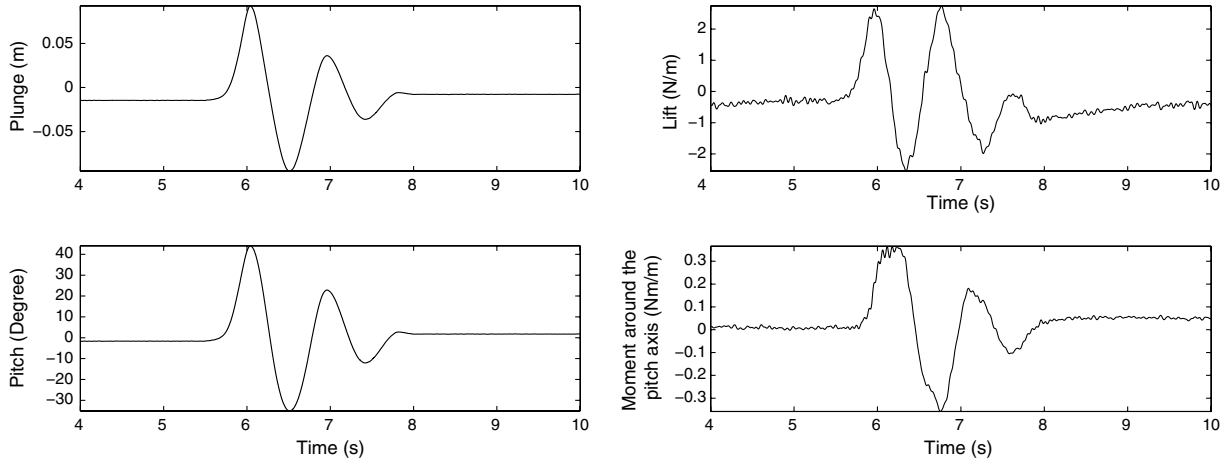

a) Pitch and plunge responses

b) Lift and moment responses

Fig. 4 Position and load response at $V = 2.5$ m/s.

approximately the same time as the maximum pitch angles. The first clear dynamic stall event is observed at $V = 3.1$ m/s, as shown in Fig. 5. The response is again highly damped and decays quickly. The pitch angle reaches a maximum of 30 deg. It should be noted that, as the excitation impulses were hand administered, they never had identical strengths. The pitching moment response at this airspeed clearly contains a double peak near the first maximum and first minimum of the pitch angle. This double peak is evidence of a sudden loss in pitching moment and subsequent recovery, a phenomenon which has been used to define dynamic stall by most authors in the field (see, for example, McCroskey and Philippe [16]).

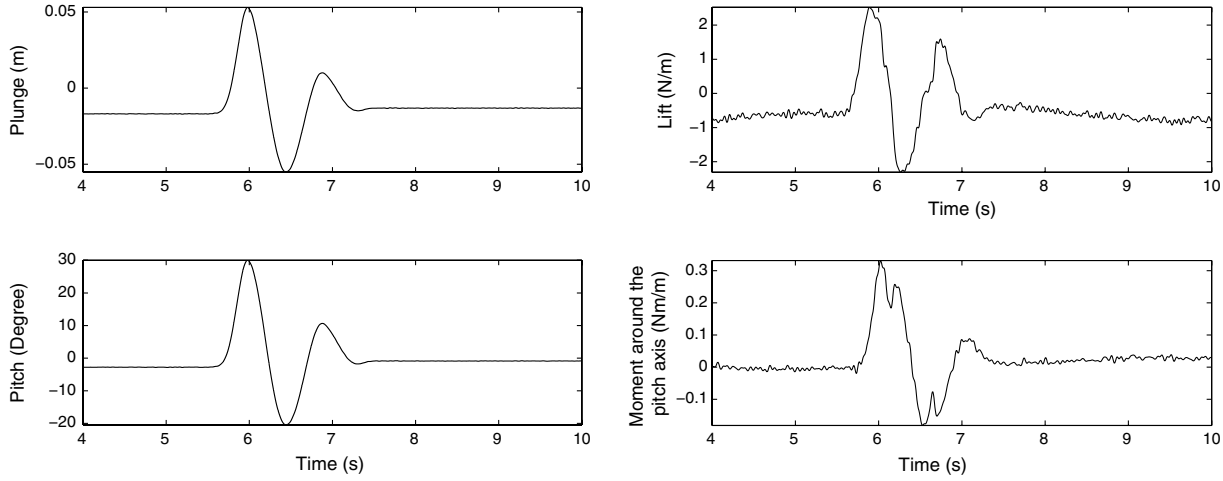

a) Pitch and plunge responses

b) Lift and moment responses

Fig. 5 Position and load response at $V = 3.1$ m/s.

It should be noted that the occurrence of dynamic stall does not necessarily coincide with stall flutter. At 3.1 m/s, the aeroelastic response is still highly damped and decays within a couple of cycles, despite the fact that dynamic stall is occurring. It must also be pointed out that the dynamic stall is more visible in the moment response than in the lift response. This can be explored further using Fig. 6, which plots the pitch, lift, and moment responses on the same axes, for $V = 2.5$ m/s and $V = 3.1$ m/s. At the 2.5 m/s airspeed, Fig. 6a, it is seen that the maximum lift occurs slightly before the maximum pitch angle, whereas the maximum moment occurs just after the maximum pitch. It can also be seen that there are undulations in the moment response near the first maximum and first minimum; these can be evidence of a weak stall event, whereby many weak vortices are released instead of a single strong one. Of course, the undulations may also be due to experimental error at such a low wind-tunnel airspeed.

On the other hand, at $V = 3.1$ m/s, there is a clear loss of pitching moment and subsequent recovery just after the first maximum and minimum pitch angles are reached. As before, the maximum and minimum lift values occur just before the extreme pitch angle values are attained. For both airspeed cases, the Reynolds numbers are quite low, 5.1×10^4 and 6.3×10^4, respectively. Very little research has been carried out on the dynamic stall phenomenon at such low Reynolds numbers. In fact, the present experiments were not specifically designed for low Reynolds numbers, and so any conclusions derived from the resulting responses are far from definitive.

It should also be mentioned that the values of the aerodynamic loads are still quite low at $V = 3.1$ m/s, in fact as low as at $V = 2.5$ m/s. This means that, at such airspeeds, the main flow component is the flow due to the pitching motion of the wing; the freestream's effect is negligible. This is no longer the case at an airspeed of $V = 8.3$ m/s, as seen in Fig. 7. The aerodynamic loads are an order of magnitude higher than in the previous airspeed cases and the motion takes much longer to decay to zero; around 3.5 cycles. It is clear that the increased aerodynamic loads have the effect of decreasing the damping. This effect is clearly due to the dynamic stall phenomenon, as both the lift and moment responses demonstrate that there are time instances at which sudden drops in values can occur. It should be noted that dynamic stall is, again, more visible in the moment response; in fact, the fundamental frequency of the moment response is twice that of the pitch or lift responses. Therefore, the dynamic stall has such a strong effect on the pitching moment around the pitch axis that, after stall, the value of the moment not only drops but it is completely reversed. Again, though, the dynamic stall phenomenon does not cause stall flutter, the responses are still decaying.

The first stall flutter event is observed at an airspeed of $V =$ 12.2 m/s. At the beginning of the motion, the wing is free to move but at rest. After the impulsive excitation is applied, though, the wing starts to perform limit cycle oscillations of amplitude 30 deg in pitch and 7 cm in plunge. It should be noted that plunge amplitude is suddenly much more significant than in the decaying response cases. This phenomenon is due to the aerodynamic coupling between pitch

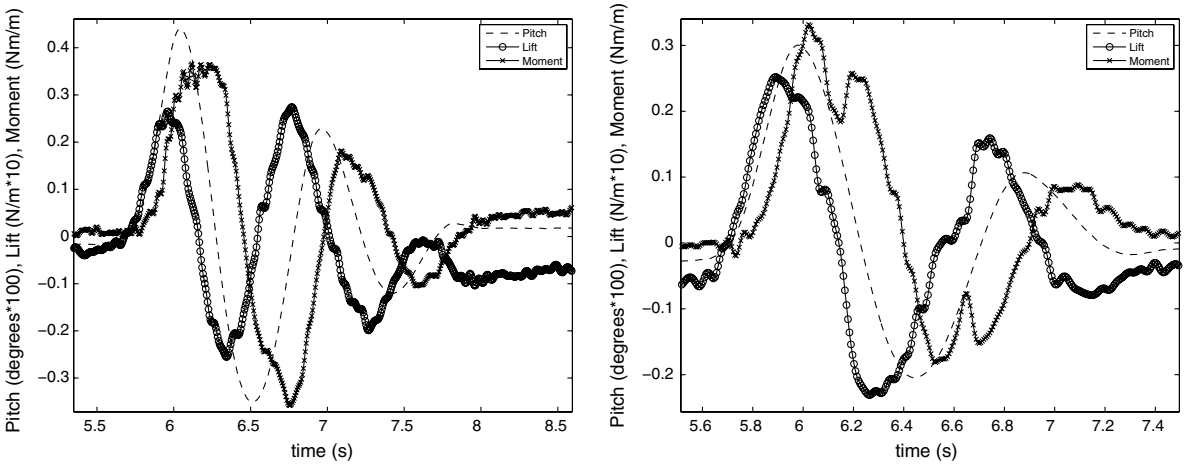

a) $V = 2.5$m/s b) $V = 3.1$m/s

Fig. 6 Pitch, lift, and moment variations at two airspeeds.

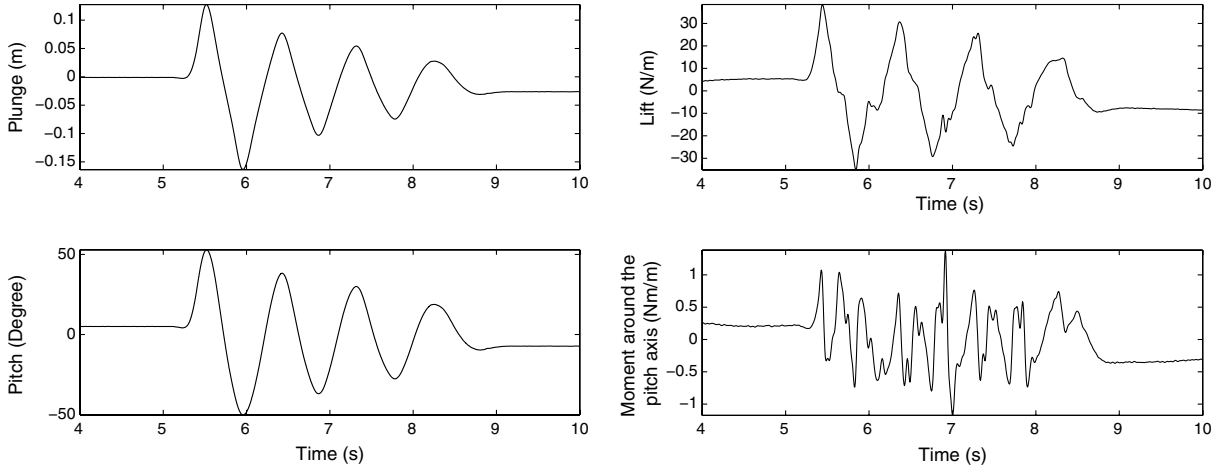

a) Pitch and plunge responses b) Lift and moment responses

Fig. 7 Position and load response at $V = 8.3$ m/s.

and plunge. Notice that the plunge responds at the same frequency as the pitch; this means that the plunge response is due to excitation by the pitch response purely. The stiffness in plunge is so much higher than the stiffness in pitch that there is no response at the plunge natural frequency. Despite the fact that the system has 2 degrees of freedom, the response is single mode.

The fact that limit cycle oscillations are possible at this airspeed means that the aeroelastic system undergoes a bifurcation at $V = 12.2$ m/s. The LCO can only be attained if a strong enough impulse is applied. Therefore, the wing's equilibrium position around zero is still stable. Such a situation corresponds to the occurrence of a subcritical bifurcation, whereby a stable focal point is encircled by an unstable limit cycle, which is in turn encircled by a stable limit cycle.

Figure 8b shows that the lift and moment responses are not very repeatable. In fact, every period of the cycle is slightly different; these differences are not stochastic, that is, they are not caused by experimental, measurement, or other errors. Several researchers in dynamic stall and stall flutter have pointed out that aerodynamic measurements can vary from cycle to cycle. Period averages of the aerodynamic response measurements over a single period have been used to create a single, average, cycle. In this work, as the aerodynamic forces affect the motion of the wing, the period averaging process has been extended to the wing displacements.

Figure 9 shows period averages for the pitch, lift, and moment responses at $V = 12.2$ m/s. Two identical periods are plotted consecutively for clarity. The pitching moment is in phase with the pitch response but the lift is completely out of phase, which may suggest that the center of pressure (i.e., the point of application of the lift) lies behind the pitching axis at all times. This situation does not occur at many airspeeds. At $V = 13$ m/s, the moment is again in phase with the lift, as seen in the period-averaged plot of Fig. 10.

Therefore, an interesting progression is observed as far as the relative phases of lift and moment are concerned with increasing airspeed:

1) In the range 0–8 m/s, the moment lags the lift by a small phase angle.

2) In the range 8–11 m/s, the moment varies at twice the frequency of the lift and, therefore, alternates between being in phase and out of phase with the lift.

3) In the range 11–12 m/s, the moment is 180 deg out of phase with the lift but in phase with the pitch response.

4) In the range 13–15 m/s, the moment is again in phase with the lift.

An interesting difference between the aeroelastic responses at $V = 12.2$ m/s and $V = 13$ m/s is the fact that, at the latter airspeed, the LCOs are self-activated, that is, there is no need for an impulsive excitation. At this airspeed, the equilibrium position is no longer stable and the wing is forced to undergo limit cycle oscillations. In more mathematical terms, the only attractor in the phase space is the stable limit cycle.

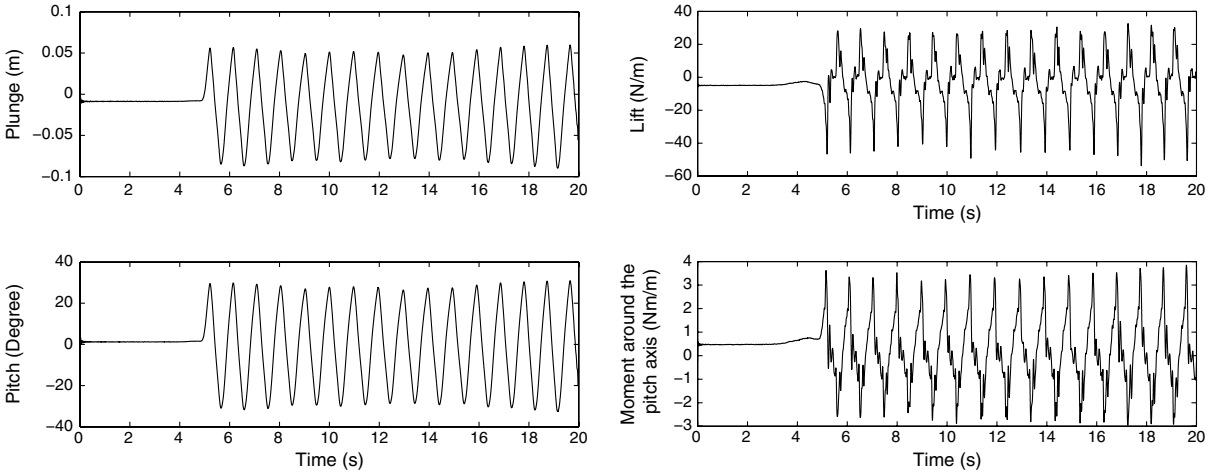

a) Pitch and plunge responses **b) Lift and moment responses**

Fig. 8 Position and load response at $V = 12.2$ m/s.

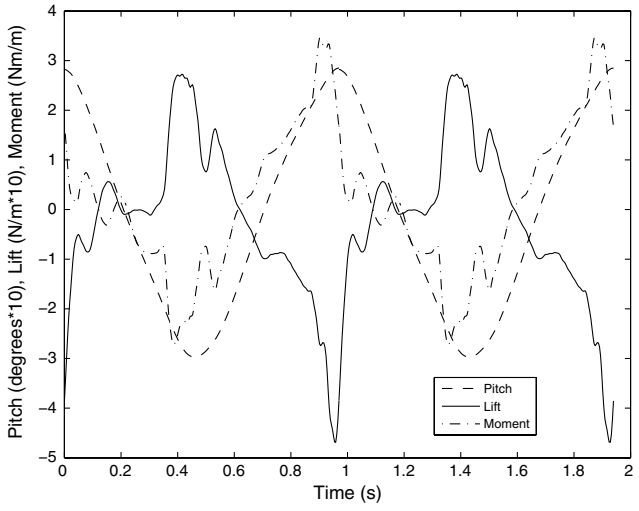

Fig. 9 Period-averaged pitch, lift, and moment variations at $V =$ 12.2 m/s.

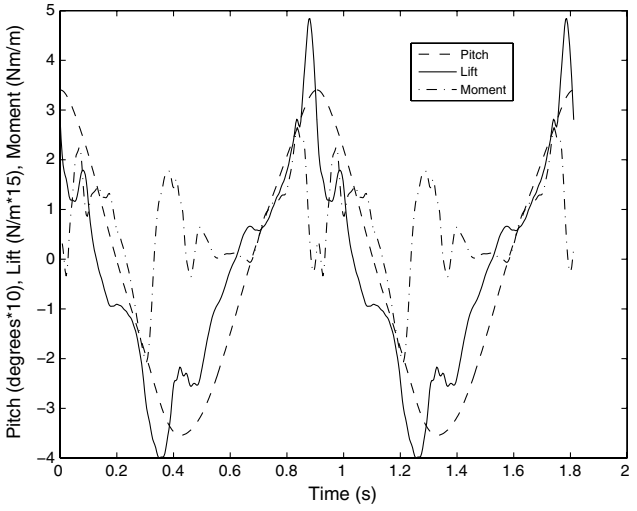

Fig. 10 Period-averaged pitch, lift, and moment variations at $V =$ 13.0 m/s.

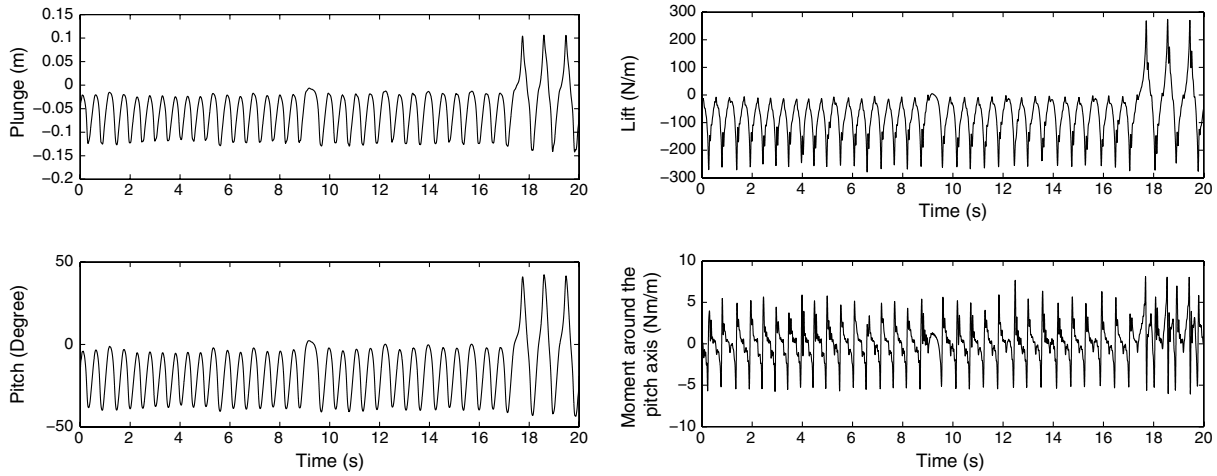

a) Pitch and plunge responses

b) Lift and moment responses

Fig. 11 Position and load response at $V = 23.7$ m/s.

As the airspeed increases, no further major changes are observed in the character of the aeroelastic and aerodynamic response of the wing. The amplitude of the oscillations increases, whereas the period decreases slightly. These changes will be described in more detail using bifurcation diagrams in the next section.

There is a qualitative change in the aeroelastic response of the wing when $V = 23.7$ m/s is reached. At this airspeed, a new bifurcation is observed. Instead of performing symmetric oscillations about the equilibrium position, the wing is performing asymmetric oscillations at negative pitch angles. However, the situation is not stable; there are some instantaneous excursions into the symmetric LCOs. In other words, the asymmetric and symmetric LCOs coexist but the asymmetric one appears to be the stronger attractor. A pitch, plunge, lift, and moment response time history at this airspeed can be seen in Fig. 11. It is obvious that the wing performs mainly asymmetric oscillations, apart from three symmetric cycles at the end of the time history. This change in aeroelastic behavior occurs very abruptly; measurements at $V = 23.2$ m/s show that the wing performs only symmetric LCOs and the pitch and plunge responses give no indication of the impending change. Mixed symmetric and asymmetric LCO responses were also encountered at the next test airspeed, $V = 25.5$ m/s. At airspeeds of $V = 26.7$ and higher (up to 29.4 m/s), only the asymmetric LCOs were observed, as seen in the pitch, plunge, lift, and moment responses of Fig. 12 for $V = 26.7$.

Both Figs. 11 and 12 demonstrate that, during the asymmetric LCOs, the lift variation is very sharp at the local minima, whereas it is quite rounded at the local maxima. Sharp changes in lift variation denote dynamic stall. As the lift minima occur near the minima of the pitch response, this suggests that dynamic stall only occurs at the pitch minima. In other words, dynamic stall only occurs on the lower surface of the wing and at high negative pitch angles. This phenomenon is in sharp contrast to the dynamic stall mechanism observed during the symmetric LCOs, whereby the flow stalls on both of the wing's surfaces.

A very similar lift variation during dynamic stall experiments is reported by Tsang et al. [17]. They present lift time responses to a prescribed pitch oscillation of an airfoil. The oscillation was centered around 15 deg and had an amplitude of 10 deg. The lift response displayed similar characteristics to the lift response of Fig. 12 where the free pitch oscillations are centered around −22 deg and have an amplitude of 20 deg. In particular, the sharpness of the lift drop at the local minima is similar to that observed by Tsang et al. at the local maxima (their oscillations were centered around a positive pitch angle). Nevertheless, it should be pointed out that the two series of experiments cannot be directly compared as the frequency of the Tsang et al. oscillations was around 4 times higher than the frequency of the present experiments. The Reynolds numbers are also different.

Although the pitch and plunge responses do not give any indications of the impending change in aeroelastic response from symmetric to asymmetric LCOs, the aerodynamic load hysteresis curves with pitch displacement can provide such an indication. Figure 13 shows the variation of lift and pitching moment with pitch displacement at four different airspeeds. The lift hysteresis curve clearly becomes progressively "pinched" in the middle until, at

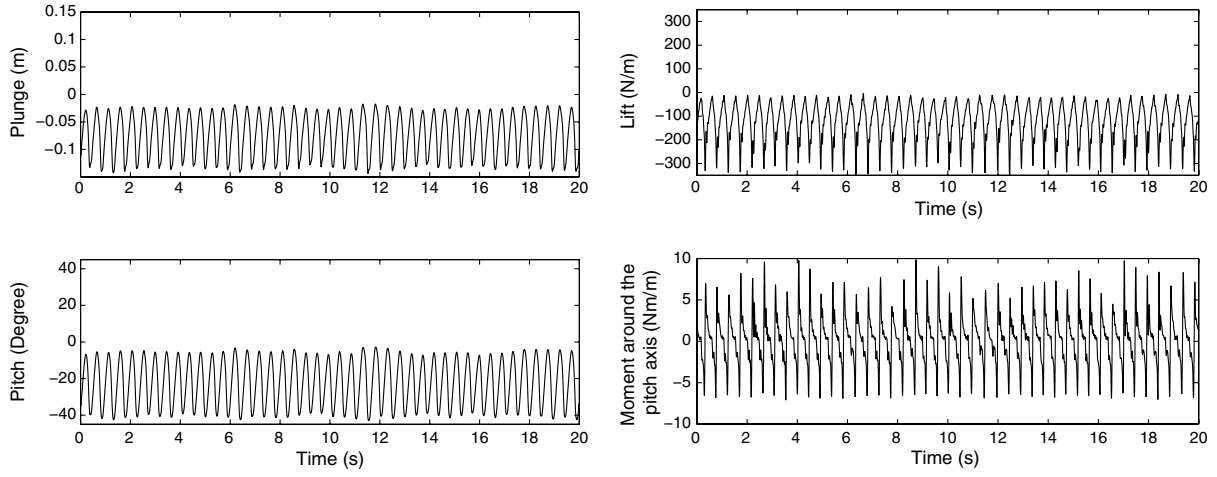

a) Pitch and plunge responses

b) Lift and moment responses

Fig. 12 Position and load response at $V = 26.7$ m/s.

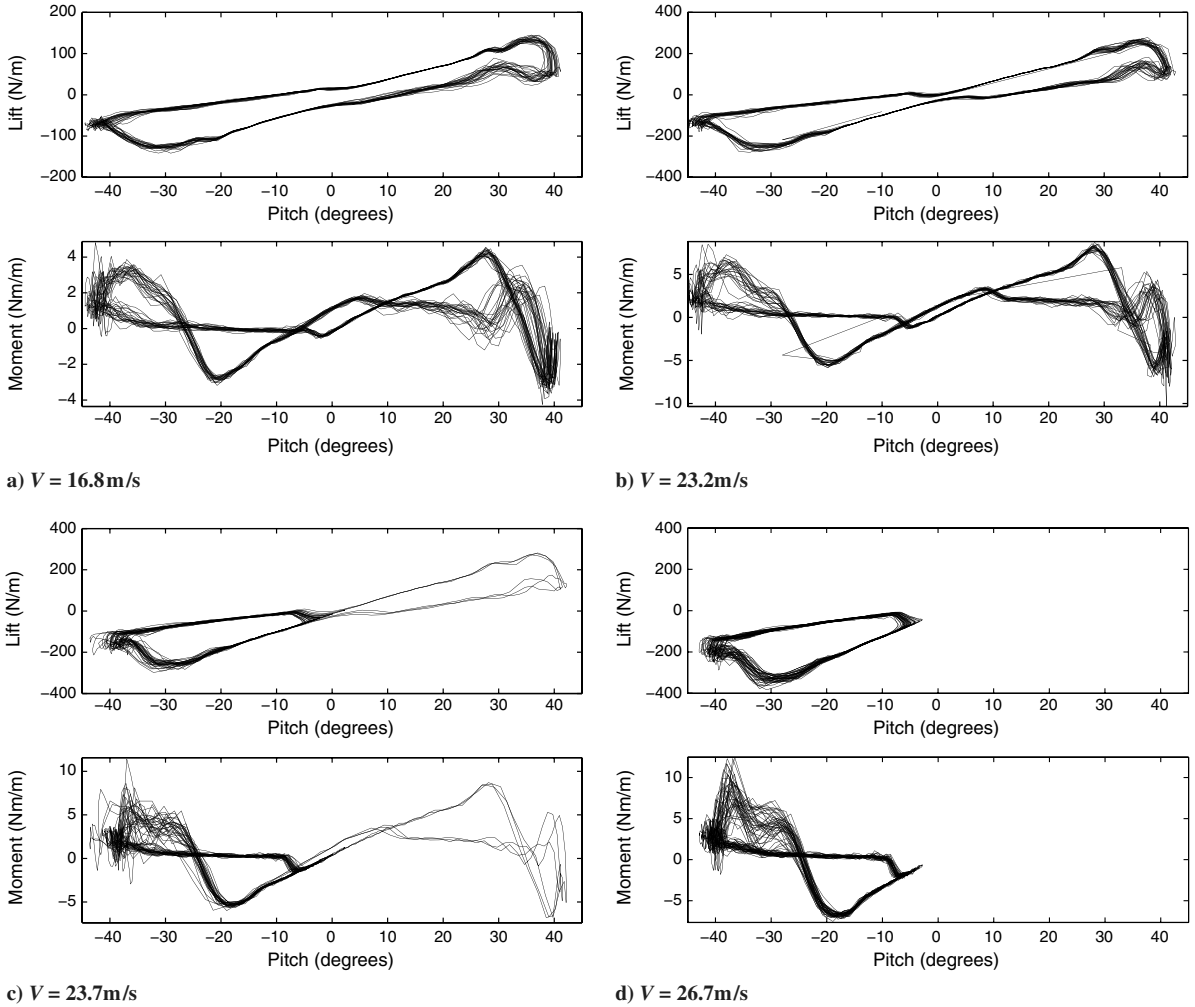

Fig. 13 Changes in aerodynamic load hysteresis curves with airspeed.

$V = 23.7$ m/s, the system begins to spend a lot more time tracing the left-hand loop than the complete hysteresis curve. At $V = 26.7$ m/s, the hysteresis has been cut completely into two loops and only the left-hand loop is traced. In other words, when the long sides of the lift hysteresis curve start touching in the middle, the intersection point belongs to three hysteresis loops; a particular lift response can follow either the symmetric or one of the asymmetric hysteresis loops. Halfman et al. [2] were the first to notice that the lift hysteresis curve becomes bow-tie shaped when dynamic stall occurs. Later on, it will be shown that the lift hysteresis and moment hysteresis curves, as plotted in Fig. 13, are only two-dimensional projections of three-dimensional curves in the space "pitch–pitch rate-lift" or "pitch–pitch rate-moment."

The pitching moment hysteresis with pitch angle features a parallelogram in its middle. This parallelogram becomes progressively thinner and longer until it becomes a single line at $V = 26.7$ m/s. Again, only the left-hand loop is traced at this airspeed and all subsequent airspeeds.

The jump from symmetric to asymmetric LCOs can be more clearly observed using period-averaged hysteresis curves. Figure 14 shows period-averaged lift coefficient hysteresis curves against pitch displacement for three airspeeds, two before and one after the bifurcation. The figures are presented in lift coefficient terms instead of lift force to clearly show how the limit cycles change with airspeed. The amplitude of the lift coefficient variation over a cycle does not change much with airspeed, at least not in the 16.8–26.7 m/s range. The only thing that changes is the fact that the two halves of the hysteresis curve get separated so that the system can only undergo oscillations in one of the two halves. The present experiments showed only oscillations in the left-hand half. It is believed that this is due to the asymmetry of the wing geometry and also to the setting of the torsion spring apparatus, which, in this case, favored a slightly negative equilibrium pitch angle; results presented later in this section will demonstrate only positive pitch angle asymmetric LCOs. It is believed that a perfectly symmetric experiment would have equal tendency to undergo the negative and positive pitch angle LCOs. The choice of limit cycle would then depend purely on initial conditions.

As mentioned earlier, at airspeeds of 23.7 and 25.5 m/s, the wing could undergo both symmetric and asymmetric limit cycle oscillations. This case needs some particular attention because bifurcation theory dictates that two stable limit cycles must always be separated by an unstable limit cycle or a homoclinic orbit (see, for example, Kuznetsov [18]). Such attractors cannot be observed experimentally (for example, unstable limit cycles are only reached when time is running backward), but their positions can be extrapolated by observing the period-averaged lift hysteresis curves of Fig. 14. A conceptual drawing of the three limit cycles can be seen in Fig. 15. The three stable limit cycles must be separated by a fourth attractor. It will be argued later that this attractor can be a homoclinic orbit in a figure eight crossing over itself at the origin.

Only negative angle symmetric LCOs were encountered during the experiments reported up to this point. In fact, it was found impossible to center the wing so that its rest position is exactly at zero pitch angle at all airspeeds. The wing was initially centered such that the rest pitch angle was slightly negative, as seen in Figs. 5a and 7a, where, after the motion has decayed, the pitch angle is negative.

The dynamic experiments were repeated with an alternative centering for the torsional springs to attempt to observe the positive pitch angle asymmetric LCO. A slightly positive equilibrium pitch angle was obtained by adjusting the winding of the torsional springs. The responses obtained with the new pitch centering were similar to those already presented up to an airspeed of 17.8 m/s. At this

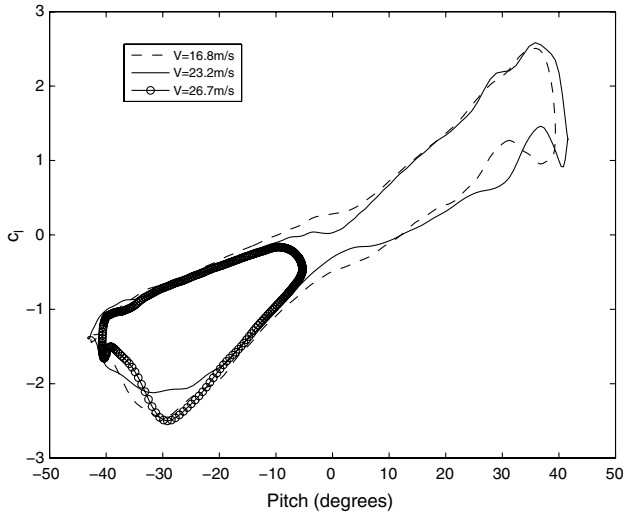

Fig. 14 Period-averaged lift hysteresis curves for three airspeeds.

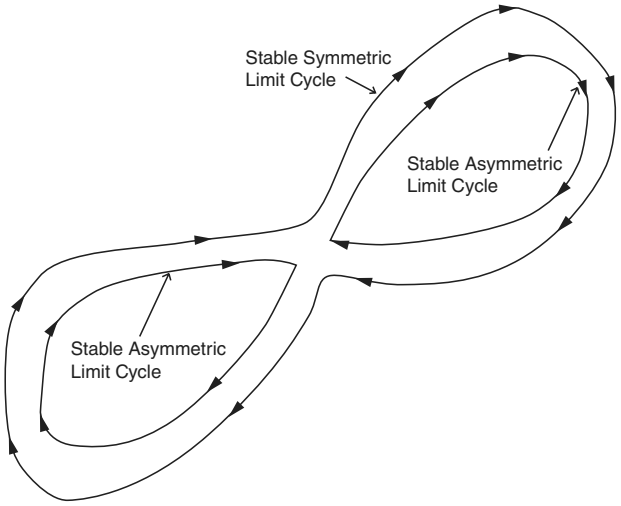

Fig. 15 Conceptual drawing of coexisting stable and unstable LCOs at $V = 23.7$ m/s.

condition, the wing started to undergo a combination of symmetric and positive angle asymmetric limit cycles oscillations, as shown in Fig. 16. The figure resembles Fig. 11 for the system with negative pitch centering at 23.7 m/s, but the asymmetric LCO occurs only at positive pitch angles. Accordingly, the lift response of Fig. 16b shows that dynamic stall only occurs on the upper surface of the wing during the asymmetric LCOs.

The symmetric LCOs disappear at an airspeed of 20.5 m/s, at which only positive angle asymmetric limit cycle responses were observed, as seen in Fig. 17. It should be noted that positive pitch centering has two effects: 1) the change in direction of the asymmetric limit cycles (positive instead of negative pitch angles), and 2) the change in airspeed at which asymmetric limit cycles first occur. With negative pitch centering, the first asymmetric LCOs occur at 23.7 m/s, whereas with positive pitch centering, asymmetric LCOs first appear at 17.8 m/s.

It has already been seen that, under negative pitch centering, the lift hysteresis curve becomes narrower in the middle until the upper and lower parts of the curve touch each other and are then split into two independent loops. This progression is also evident in the case of positive pitch centering, although less clearly. Figure 18 shows period-averaged lift coefficient hysteresis curves for four airspeeds, two before the asymmetric LCO bifurcation and two after. It can be seen that the symmetric lift hysteresis curve becomes narrower in the middle as the airspeed is increased but never to the point of touching, as in the negative pitch centering case. The symmetric lift hysteresis curve at $V = 17.8$ m/s does not have a figure-eight shape, yet asymmetric limit cycles are possible at this airspeed. Therefore, a figure-eight-shaped (or bow-tie shaped, as described by Halfman et al. [2]) lift hysteresis curve is not a necessary condition for the bifurcation to asymmetric LCOs.

In fact, the eight-shaped lift hysteresis curves in Figs. 13 and 14 are slightly misleading. The figures are 2-D projections of 3-D curves. Figure 19 plots the lift coefficient hysteresis curves against pitch and pitch rate in 3-D space, for negative pitch centering at 23.7 m/s and positive pitch centering at 17.8 m/s. It can be seen that neither of the cases features a figure-eight shape, although they both demonstrate a narrowing in the middle, around the $\alpha = 0$ line, where α is the pitch angle. These plots are important because they demonstrate that there is no qualitative change in the dynamic stall mechanism occurring due to the change in pitch centering; both results come from essentially the same system. A figure-eight shape appears in the 2-D projection of the lift hysteresis curve of the negative pitch centered system purely as a result of a slightly different orientation of the plane on which the curve lies. This difference in orientation is probably due to the slight asymmetry of the stall flutter wing, which has already been discussed several times. Figures 19c and 19d show that the pitching moment coefficient hysteresis curves are similar to the lift hysteresis curves but the plane on which they lie is strongly curved and not approximately flat, as is the case with the lift hysteresis. Therefore, the pitching moment demonstrates a much more complex dependence on pitch rate.

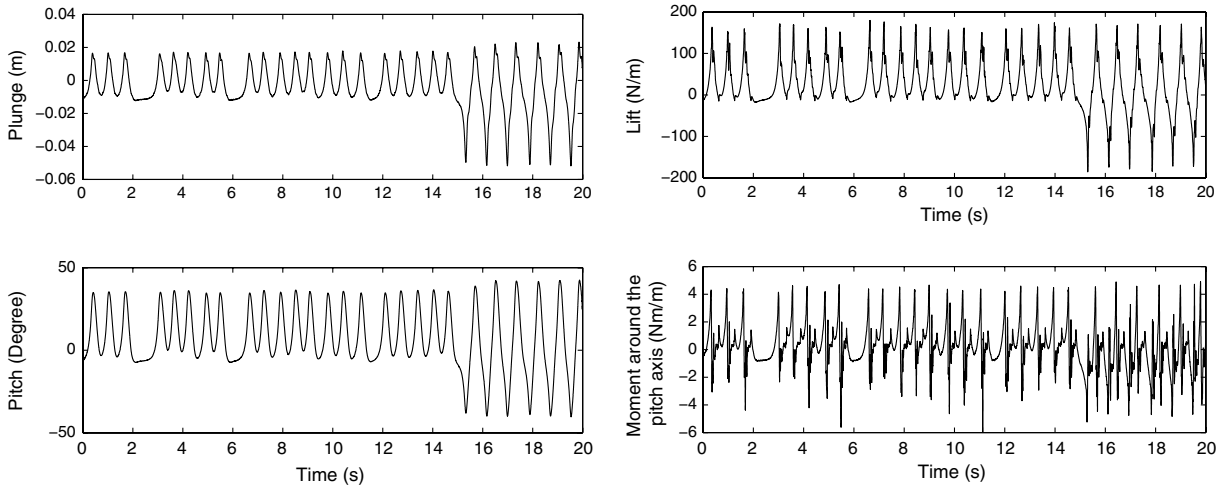

a) Pitch and plunge responses **b) Lift and moment responses**

Fig. 16 Position and load response at $V = 17.8$ m/s with positive pitch centering.

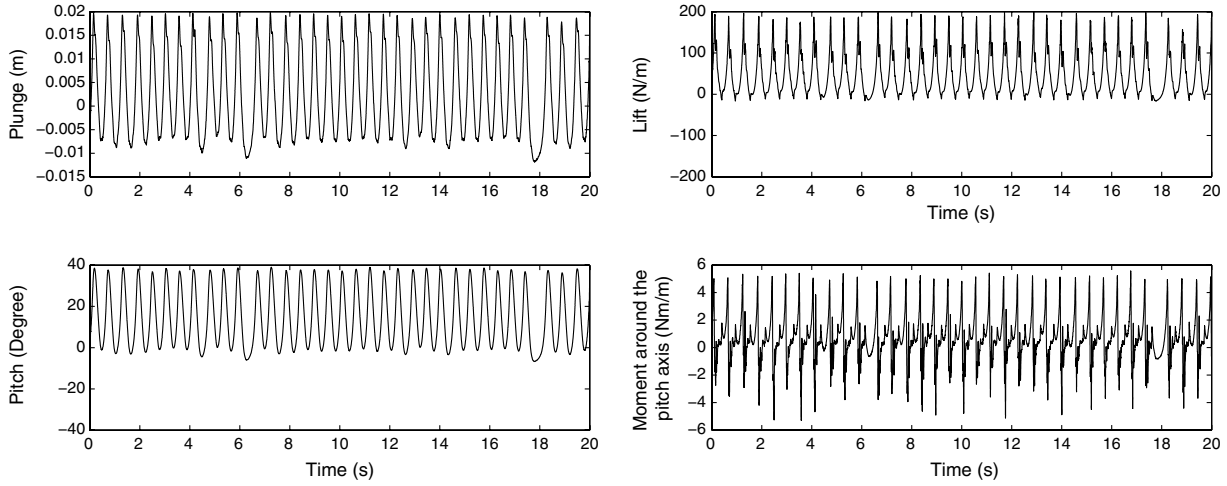

a) Pitch and plunge responses **b) Lift and moment responses**

Fig. 17 Position and load response at $V = 20.5$ m/s with positive pitch centering.

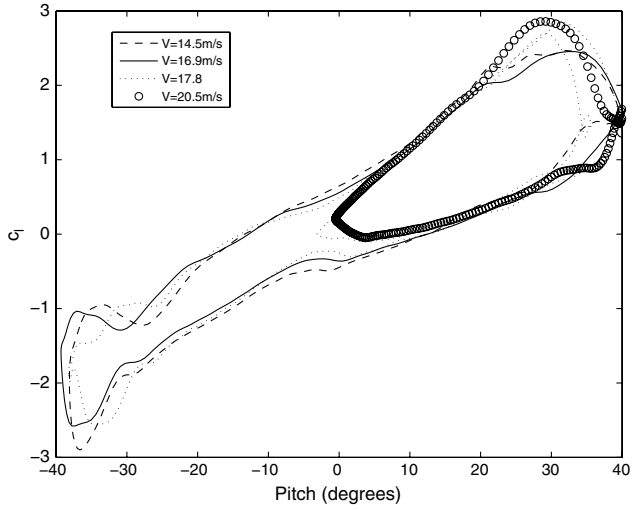

Fig. 18 Period-averaged lift hysteresis curves for three airspeeds, positive pitch centering.

The occurrence of the various types of LCO for the stall flutter wing will be further analyzed and tentative explanations will be proposed in the next section, using bifurcation analysis.

V. Bifurcation Behavior

Despite the complexity of the present experimental wing system, its equations of motion can be written in the simple first-order form:

$$\dot{\mathbf{x}} = \mathbf{f}(\mathbf{x}, \mathbf{w}) \tag{1}$$

where $\mathbf{x}$ is the vector of system states, which includes both structural and aerodynamic states, $\mathbf{f}$ is a vector of nonlinear functions, and $\mathbf{w}$ is a vector of system parameters, such as airspeed, structural stiffness, etc. Strictly speaking, dynamic systems involving unsteady aerodynamic loads are infinite dimensional, that is, the number of states is infinite [19]. The aerodynamic loads depend not only on the current value of the states but also on all previous values, due to the effect of the wake vorticity. In practice though, only the wake vorticity close to the wing has a measurable effect on the aerodynamic loads. Therefore, the system is approximately finite dimensional; vorticity shed a long time ago can be neglected.

As the equations of motion are nonlinear, they can have more than one solution; therefore, several solutions can coexist at any set of parameter values. A change from one type of solution to another as a parameter is varied is termed a bifurcation [20]. It can also be said that a bifurcation is the intersection of one solution branch with another solution branch [21].

The local bifurcation behavior of the stall flutter wing as the airspeed is changed can be described using the following cases:

1) For $V < 12$ m/s, the response is oscillating decaying.

2) For $12 \leq V < 13$ m/s, the response is oscillating decaying or symmetric LCO.

3) For $13 \leq V < 18$ m/s, the response is symmetric LCO.

4) For $18 \leq V < 27$ m/s, the response is asymmetric LCO or symmetric LCO. The first positive pitch asymmetric LCOs appear at 17.8 m/s, the first negative pitch asymmetric LCOs at 23.7 m/s.

5) For $V > 27$ m/s, the response is symmetric LCO. Symmetric LCOs for the positive pitch centered wing disappear at 20.5 m/s. For the negative pitch centered wing they disappear at 26.7 m/s.

Cases 1–4 are plotted in the α–$\dot{\alpha}$ phase plane in Fig. 20. The shapes of the LCOs are taken from the experimental α vs $\dot{\alpha}$ data. In Fig. 20a (case 1), the only singularity in the phase plane is the stable spiral point. The observed trajectory clearly shows the spiral effect produced by the singularity. The trajectory begins at the far right end of the plot and spirals inward toward the fixed point.

For case 2, two trajectories are plotted in Fig. 20b. Trajectory 2 tends toward the stable spiral point as before. This trajectory is the result of a weak externally applied impulse. Trajectory 1 in Fig. 20b is a limit cycle oscillation. It is the result of a stronger impulsive excitation. In the 12–13 m/s airspeed range, it is possible to observe a hysteretic phenomenon whereby the response is decaying as the airspeed is increased toward 13 m/s, becomes suddenly LCO as 13 m/s is exceeded, and remains LCO as the airspeed is decreased and until it drops below 12 m/s.

Figure 20c corresponds to case 3. Only one trajectory is plotted, the limit cycle oscillation. Finally, for case 4, three orbits are plotted in Fig. 20d: the symmetric limit cycle, the positive pitch asymmetric limit cycle, and the negative pitch asymmetric limit cycle. At certain airspeeds, a single trajectory can jump from the asymmetric limit cycle to the symmetric one and vice versa, as shown in Fig. 11. Case 5 is not represented in these drawings because it features only one of the two asymmetric limit cycles of Fig. 21d.

The observations of Fig. 20 are presented in conceptualized form in Fig. 21 to pinpoint the location and stability of the various singularities in the phase space. The shape of the unstable limit cycle and homoclinic orbit as well as the positions of the unstable fixed points are, of course, qualitative only. Initially, the only singularity to exist in the phase plane is the stable focal point (Fig. 21a). Then, a stable and an unstable limit cycle come into existence at an infinitesimal distance from each other but at a finite distance from the focal point. As the airspeed is increased, the stable and unstable limit cycles move away from each other. The stable LCO amplitude increases, whereas that of the unstable LCO decreases (Fig. 21b). Eventually, the unstable limit cycle becomes so small that it merges

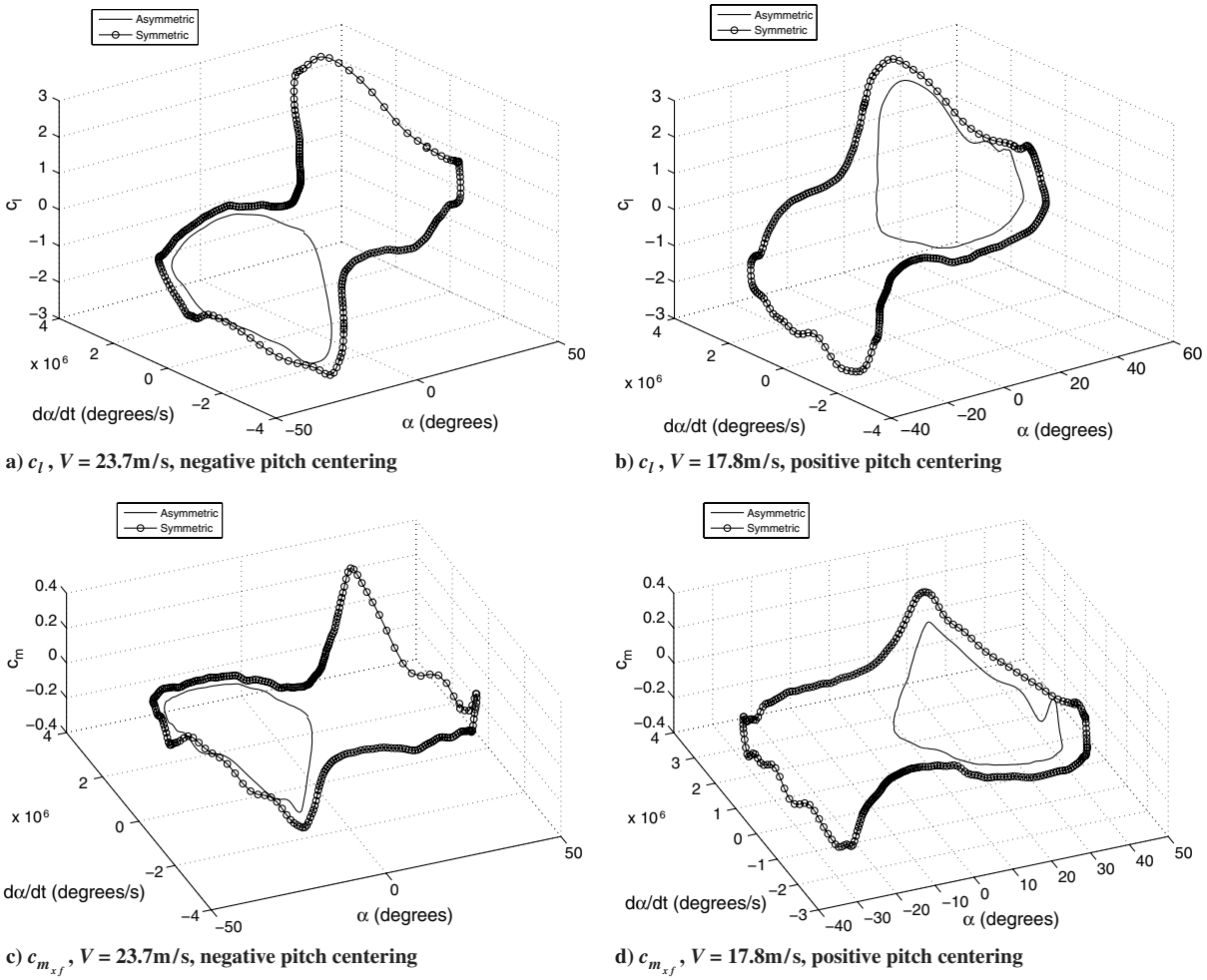

a) c_l, V = 23.7m/s, negative pitch centering

b) c_l, V = 17.8m/s, positive pitch centering

c) $c_{m_{xf}}$, V = 23.7m/s, negative pitch centering

d) $c_{m_{xf}}$, V = 17.8m/s, positive pitch centering

Fig. 19 Three-dimensional lift and pitching moment hysteresis curved for positive and negative pitch centering.

with the focal point to become an unstable focal point; only a stable LCO motion is now possible (Fig. 21c). Finally, the focal point becomes a saddle point through which passes a double-loop homoclinic orbit; two unstable focal points are also created at either side of the saddle point on the $\dot{\alpha} = 0$ axis. The homoclinic orbit splits the phase plane into three different regions, in each of which a stable limit cycle can exist (Fig. 21d).

The first bifurcation to be observed as the airspeed is increased from zero is a fold (also known as saddle-node) bifurcation. This bifurcation involves the sudden appearance of a saddle point in the phase plane and the subsequent separation of this saddle into a stable and an unstable node. Although this is a bifurcation of fixed points only, there exists an analogous fold (or saddle-node) bifurcation of limit cycles [18]. A half-stable limit cycle appears out of nowhere in the phase-parameter space and then branches off into a stable and an unstable limit cycle. Case 2 therefore corresponds to the instance where the stable and unstable limit cycles have already branched off. Figure 22a is a drawing of a fold bifurcation.

The second bifurcation to be observed is a subcritical Hopf bifurcation. During such a bifurcation, the stability of a fixed point changes from stable focus to unstable focus, and an unstable limit cycle begins to grow around it for decreasing values of the parameter. At the exact parameter value for which the bifurcation occurs (the Hopf point), the Jacobian of the system has a pair of purely complex conjugate eigenvalues. Figure 22b shows a drawing of a subcritical Hopf bifurcation followed by a fold bifurcation of limit cycles. It is a generic plot of limit cycle amplitude against parameter value. At a parameter value of zero, an unstable limit cycle starts to grow in the direction of decreasing parameter value. At a parameter value of -1.8, the unstable limit cycle changes direction and becomes stable. The parameter range at which the unstable limit cycle exists corresponds to the range $12.2 \leq V < 13.0$ m/s for the stall flutter wing, where both LCOs and decaying responses can be observed.

The fold and Hopf bifurcations are sufficient to explain the response of the stall flutter wing in cases 1, 2, and 3. Such bifurcations are frequently encountered in aeroelastic systems. The fold bifurcation is also known as fold catastrophe exactly because it appears abruptly and without warning; see, for example, Jordan and Smith [22].

The bifurcation resulting in case 4 is less common. It is clearly a symmetry-breaking bifurcation, leading to the formation of a homoclinic figure-eight unstable orbit. The unstable equilibrium point at the origin is split into two unstable foci lying inside the stable asymmetric limit cycles and a saddle lying at the node of the figure-eight homoclinic orbit.

The occurrence of such a homoclinic orbit is described by Kuznetsov [18] and Guckenheimer and Holmes [23], occurring on the generalized Duffing oscillator. To describe the bifurcation leading up to the creation of such an orbit, Kuznetsov uses the rather obvious term "homoclinic figure-eight" bifurcation [18]. It is a two-parameter bifurcation, depending on a damping parameter and a stiffness parameter. In the case of the stall flutter wing, the bifurcation also depends on two parameters. The damping-related parameter is the airspeed which, when reaching a critical value, can induce aerodynamic loads such that the effective damping is negative. The stiffness-related parameter is the stiffness of the torsional springs. More details will be given on these parameters in the next subsection where a physical explanation of the bifurcations will be attempted.

Here is a proposed list of the bifurcations undergone by the stall flutter wing investigated here:

1) Between cases 1 and 2 is a fold bifurcation: an unstable limit cycle growing in amplitude in the direction of decreasing airspeed reverses direction and becomes stable.

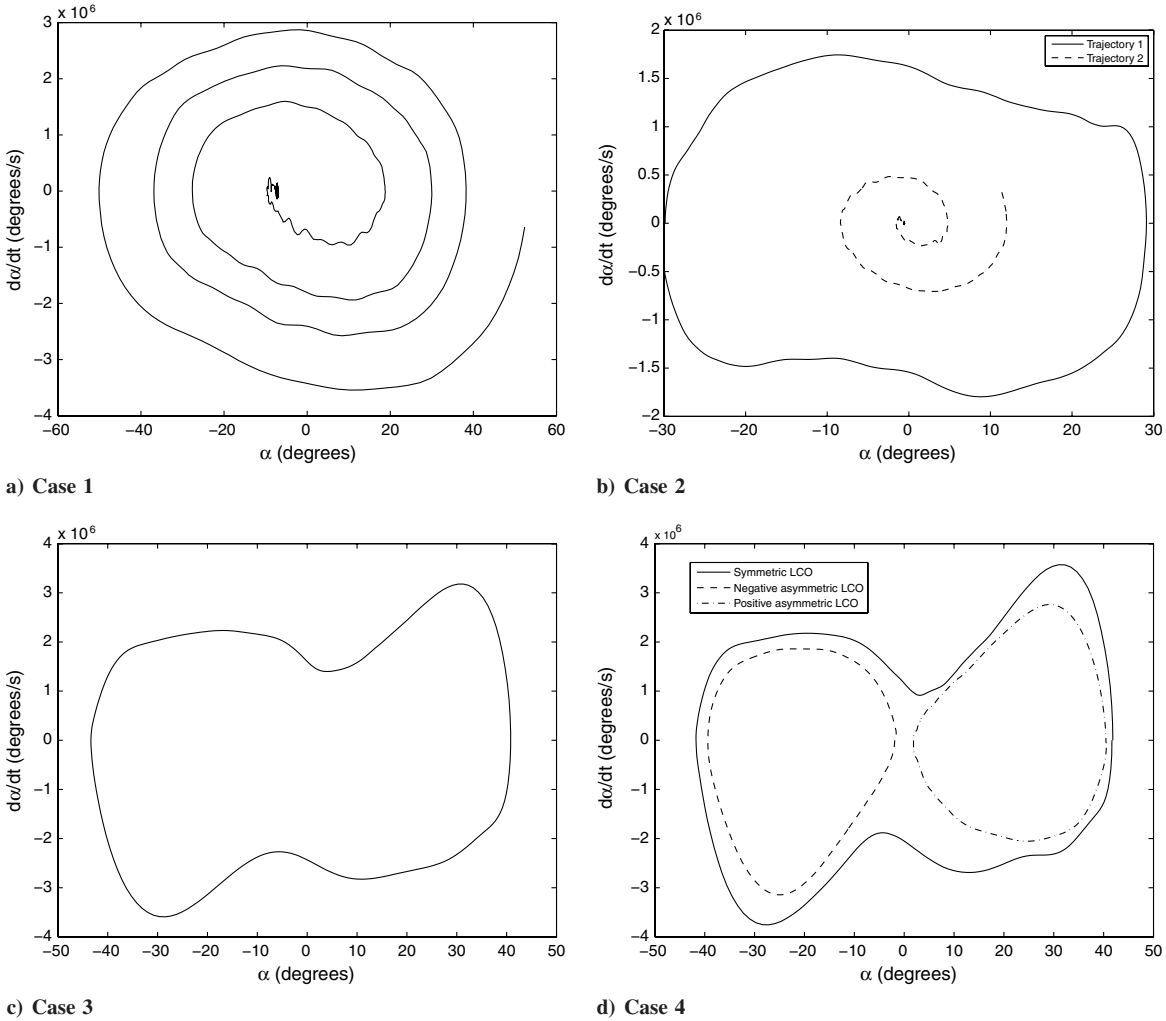

a) Case 1

b) Case 2

c) Case 3

d) Case 4

Fig. 20 Changes in measured trajectories with airspeed.

2) Between cases 2 and 3 is a subcritical Hopf bifurcation: a stable spiral point becomes unstable and the linearized system in the neighborhood of the bifurcation has a pair of purely complex eigenvalues.

3) Between cases 3 and 4 is an unstable figure-eight homoclinic bifurcation: an unstable spiral point becomes a saddle point and two new unstable spiral points are created either side of it. A homoclinic figure-eight orbit is created, enclosing two stable limit cycles around the two new unstable spiral points.

The three bifurcations affecting the stall flutter wing result in the variation of limit cycle amplitude and frequency. These variations can be conveniently displayed using a bifurcation diagram, which plots the maxima and minima of the system responses as a function of governing parameter, in this case airspeed. Figure 23 shows bifurcation diagrams for the pitch, plunge, lift, and moment LCO amplitudes. These diagrams were obtained using period-averaged responses and plot the extremes (maximum and minimum) of the observed LCOs at each airspeed. The most important conclusion to be drawn from these graphs is that the major changes in LCO amplitude and frequency occur at airspeeds between 12 and 15 m/s. After 15 m/s, the LCO amplitudes remain approximately constant until the homoclinic bifurcation; at that point, the limit cycle becomes asymmetric and its amplitude is halved. Subsequently, the asymmetric LCOs move away from the origin with increasing airspeed but the LCO amplitude does not vary much.

Another interesting observation concerning Fig. 23 is related to the amplitudes of the lift coefficient. It can be seen that the highest lift coefficient values are nearly three, that is, almost 3 times higher than the maximum static lift coefficients presented in Fig. 3a. This is a very well-known phenomenon associated with dynamic stall; the maximum instantaneous lift coefficient can significantly exceed the maximum static lift coefficient, whereas the maximum instantaneous pitch angle can significantly exceed the static stall angle.

Figure 24 shows the variation of the LCO period with airspeed. At airspeeds less than 12 m/s, the LCO period is represented by zeros as there is no periodic response. It can be seen that the LCO period is initially very close to one but drops to around 0.85 between 12 and 15 m/s. Subsequently, it remains constant until the homoclinic bifurcation. The period of the asymmetric limit cycle is significantly smaller than that of the symmetric one and keeps dropping as the airspeed is increased. It is interesting to note that, although the periods of the symmetric limit cycles are equal for the two configurations, the period of the positive pitch angle LCO is slightly lower than that of the negative pitch angle LCO. It can be concluded that the wing's slight asymmetry causes the two asymmetric LCOs to have slightly different periods (and therefore frequencies).

A. Physical Justification of Bifurcations

The bifurcation analysis of the previous subsection describes in detail the mathematical phenomena behind the aeroelastic response of the stall flutter wing. Nevertheless, it does not constitute a physical description of the phenomenon. Here, tentative explanations of the bifurcation behavior of the stall flutter wing will be proposed, using physical mechanisms.

The stall flutter wing is subjected to two major bifurcations. The first one is the subcritical Hopf, followed by the fold. The second is the homoclinic figure-eight bifurcation. It is proposed that the Hopf and fold bifurcations are caused by the dynamic stall phenomenon whereas the homoclinic bifurcation by static divergence.

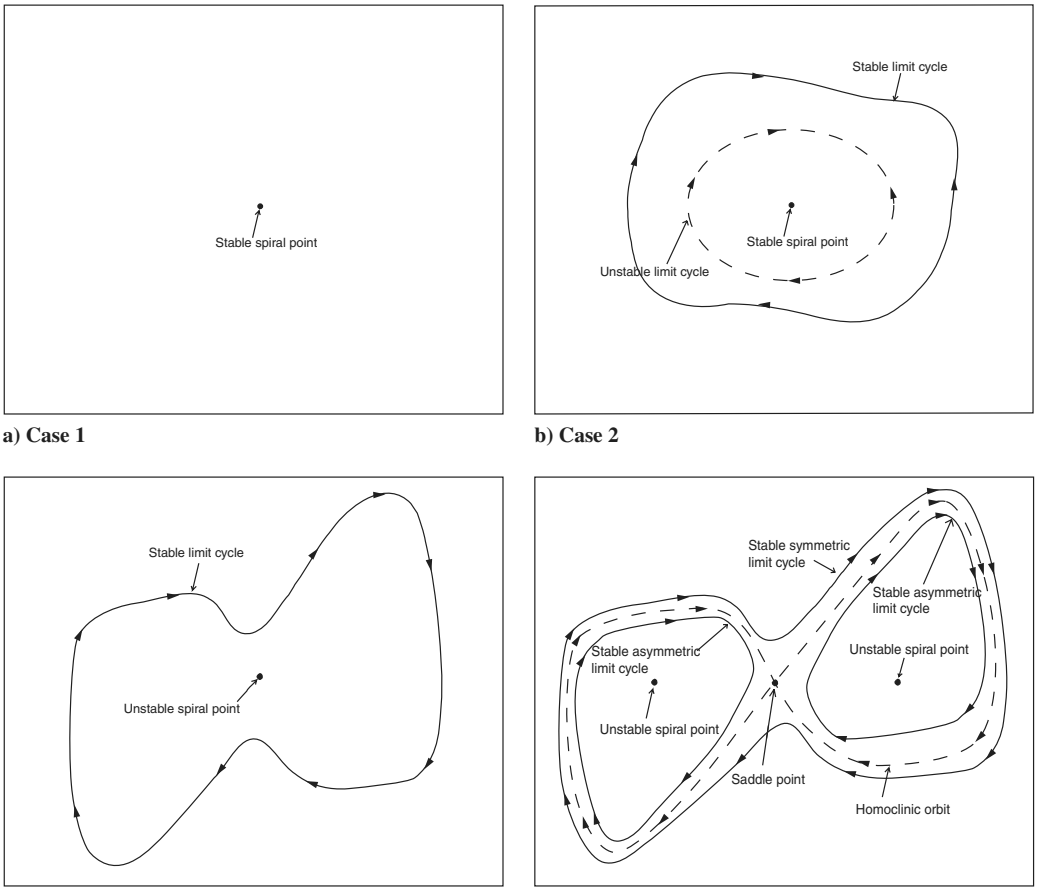

a) Case 1 **b) Case 2**

c) Case 3 **d) Case 4**

Fig. 21 Conceptualized changes in limit cycle position and stability with airspeed.

As mentioned in the Introduction, several authors have identified the fact that stall flutter is caused by negative damping introduced by the dynamic stall. Of course, this statement is a simplification of the phenomenon because the damping in the stall flutter wing is nonlinear. In this work, the work done by the aerodynamic loads is used to justify the occurrence of the Hopf and fold bifurcations.

As the plunge degree of freedom was found not to participate in the stall flutter mechanism, only the work done on the pitch degree of freedom will be considered here. The work done by the flow on the pitch depends uniquely on the pitching moment around the pitching axis. The incremental work done by the pitching moment as the pitch angle increases by a small amount $\delta\alpha$ is given by

$$\delta W = M_{xf}\delta\alpha \tag{2}$$

where M_{xf} is the pitching moment around the pitch axis. When δW is positive, then work is done by the fluid on the wing. When it is negative, then the wing does work on the fluid. The total work done during a complete period of decaying or LCO response is given by

$$W = \oint_T \delta W \tag{3}$$

where, in the case of decaying oscillations, T is the time between two successive maxima of the pitch response, whereas, in the case of

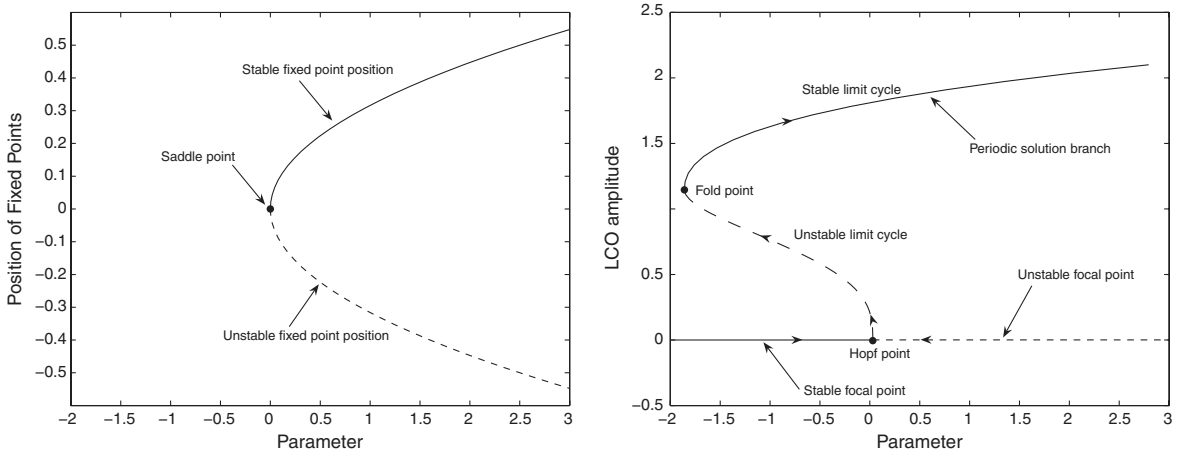

a) Fold bifurcation **b) Subcritical hopf and fold**

Fig. 22 Bifurcation drawings: a) fold, and b) subcritical Hopf followed by fold.

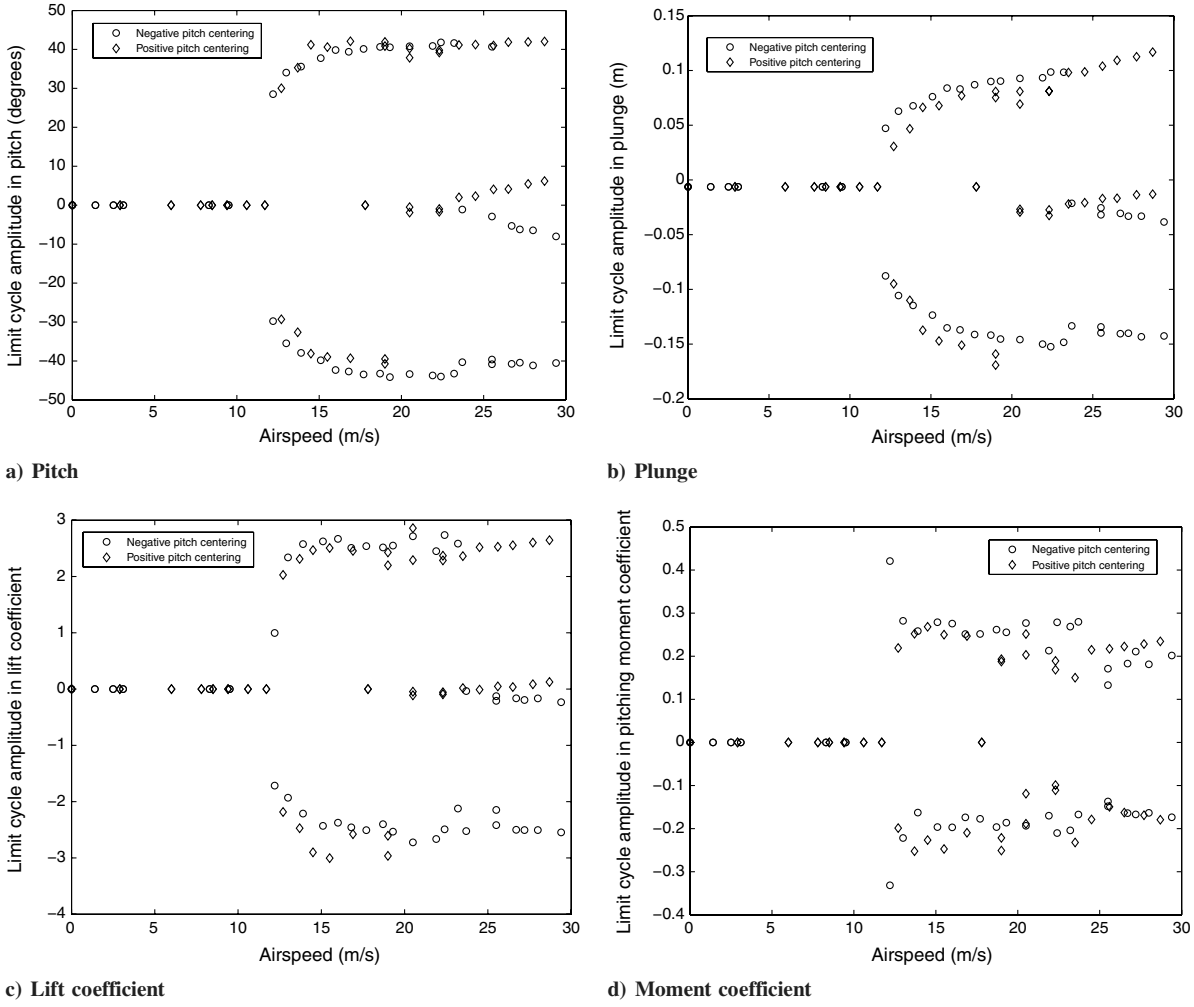

a) Pitch **b) Plunge**

c) Lift coefficient **d) Moment coefficient**

Fig. 23 Bifurcation diagrams.

LCOs, T is the period of the limit cycle oscillations. In practice, the total work done over a period can be calculated by summing all the δW calculated over a period, that is

$$W = \sum_{i=1}^{n} M_{xf_i}(\alpha_i - \alpha_{i-1}) \tag{4}$$

for $i = 0, \ldots, n$, where n is the total number of time instances measured in a period.

The total work done by the fluid on the wing over a period is plotted in Fig. 25 for the configuration with negative pitch centering. Both pre- and postbifurcation data are included. It can be seen that the work done at prebifurcation airspeeds ($V < 12$ m/s) is negative, that is, the wing is doing work on the fluid. This situation is logical, as the motion is decaying, therefore the wing must loose energy.

At postbifurcation airspeeds, the total work done by the fluid on the wing is positive, which indicates that the wing is gaining energy. However, the work done by the fluid on the wing over a period must

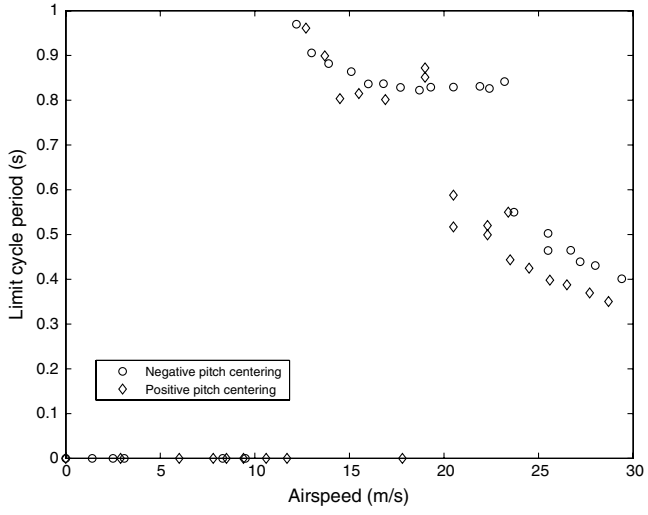

Fig. 24 LCO period variation with airspeed.

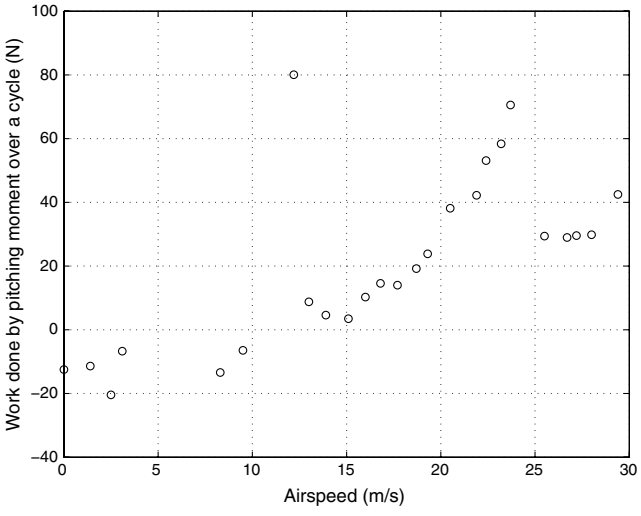

Fig. 25 Total work done by the fluid on the wing over a period.

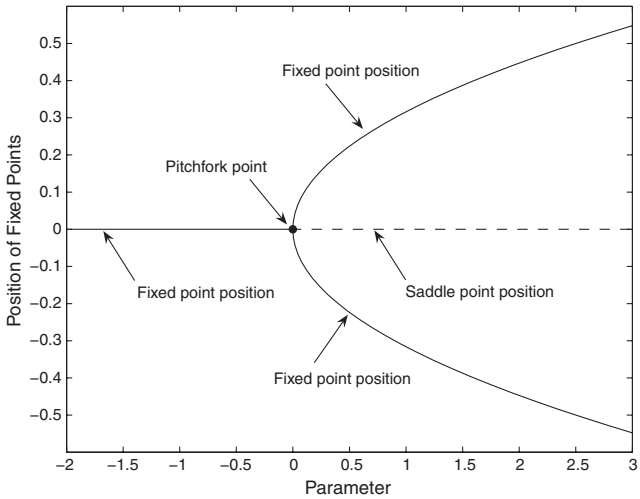

Fig. 26 Pitchfork bifurcation.

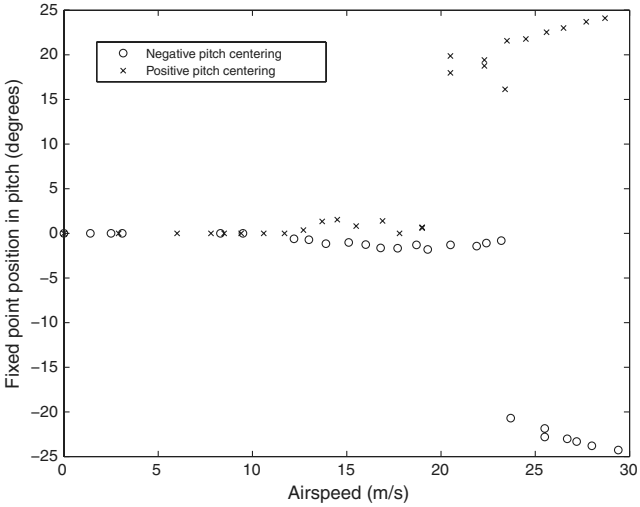

Fig. 27 Conceptual and measured imperfect pitch bifurcations.

be equal to the energy lost by the wing via other mechanisms such as friction, so that the amplitude of oscillation never increases or decreases; having said that, there are small period-to-period variations, but the results presented in Fig. 25 are period averaged. It should be noted that the amount of work done by the fluid increases with airspeed until the second bifurcation when the asymmetric LCOs start occurring. Then, the total work done is almost halved and stays constant up to an airspeed of nearly 30 m/s. Also note that the amount of work done at $V = 12.2$ m/s, that is, the earliest LCO measured, is very high compared to the work done at subsequent airspeeds. It is not known why this is the case. At this particular airspeed, both LCO responses and decaying responses are possible. When the wing is disturbed from its fixed point, if the disturbance is high, then the wing will start absorbing energy from the fluid. If the initial disturbance is low, then the wing will loose energy to the fluid. The only difference between these two cases is that, in the former, the instantaneous pitch angle and pitch rate become high enough to activate the stall flutter mechanism. Low disturbances cannot activate this mechanism. As the airspeed is increased, smaller and smaller disturbances are required to set the dynamic stall phenomenon in motion.

It can be concluded that the subcritical Hopf and fold bifurcations are caused by dynamic stall. During dynamic stall, enough work is done by the fluid on the wing to cause the wing to undergo limit cycle oscillations, that is, stall flutter.

Static divergence is a static aeroelastic phenomenon which occurs when the aerodynamic forces overcome the structural restoring forces. For the 2-D airfoil equations of motion, the static divergence condition in pitch is obtained when

$$K_\alpha \leq \rho U^2 e c^2 \pi \tag{5}$$

The corresponding airspeed, $U_{\text{div}} = \sqrt{K_\alpha / \rho e c^2 \pi}$, is the static divergence speed. At divergence, an aeroelastic system's fixed point becomes a saddle point. The total stiffness in pitch K_α of the stall flutter wing is 14.5 $\text{N} \cdot \text{rad}^{-1} \cdot \text{m}^{-1}$. Therefore, the static divergence airspeed is $U_{\text{div}} = 17.7$ m/s.

The first positive pitch angle asymmetric LCOs appear at 18.1 m/s, that is, just past the static divergence airspeed. This is no coincidence; it is believed that the homoclinic bifurcations that give rise to the asymmetric LCOs are in fact caused by static divergence. The figure-eight-shaped homoclinic orbit and the division of the phase space into three areas is the result of the interaction of the static divergence and dynamic stall phenomena. Static divergence is a pitchfork bifurcation, drawn conceptually in Fig. 26, involving the transformation of a node or spiral point into a saddle point and the creation of two new nodes or spiral points at each side of this saddle point [22]. Such a transformation, combined with the existence of a stable limit cycle, leads to the creation of the homoclinic figure-eight orbit. The particular bifurcation encountered here is a subcritical pitchfork, involving the transformation of an unstable fixed point to a saddle and two new unstable fixed points [24,25].

Of course, it should be remembered that the first negative pitch angle LCOs appear at significantly higher airspeeds, almost 24 m/s. The mismatch between the occurrences of positive and negative angle asymmetric LCOs is believed to be due to the asymmetry of the wing. The pitchfork bifurcation is, in fact, an imperfect pitchfork, which can occur in systems with imperfections such as a slight asymmetry [26]. Figure 27 shows the imperfect pitchfork bifurcation actually measured from the stall flutter wing. It is an approximation, as the fixed point positions were taken to be the midpoints of the LCOs. The mean LCO amplitudes $|\max(\alpha) + \min(\alpha)|/2$ are plotted at each test airspeed for the positive and negative equilibrium pitch angle configurations.

B. Dynamic Stall Mechanism

In this subsection, the variation of the pressure distributions during a LCO cycle will be presented to investigate the dynamic stall phenomenon. Two representative response cases are considered: a symmetric LCO at $V = 23.2$ m/s and an asymmetric LCO at $V = 26.7$ m/s.

Figure 28 plots the pressure distributions around the airfoil during a dynamic stall event on the upper surface at $V = 23.2$ m/s. The upper and lower surface pressure coefficients are plotted against the chordwise position at 18 different instances in time. The title of each plot gives the corresponding instantaneous pitch angle.

1) At $\alpha = 18.2$ deg, the flow is completely attached around the airfoil and the instantaneous lift coefficient is 1.17. In fact, the flow is attached even though the pitch angle is much higher than the static stall angle of attack; this is due to the motion itself.

2) At the next snapshot, $\alpha = 22.9$ deg, the flow is probably still attached but there is a significantly higher suction peak near the leading edge, giving a lift coefficient of 1.54.

3) At $\alpha = 25.1$ deg, the suction peak is even stronger and has spread downstream to almost the quarter-chord; the instantaneous lift coefficient is 1.70.

4) At $\alpha = 27.6$ deg, the suction peak has stopped increasing in strength but has expanded further downstream to almost the third-chord; the lift coefficient has reached a value of 2.08.

5) The snapshot at $\alpha = 30.2$ deg is quite interesting because the suction peak is still present but there is a dent in it, which suggests that it has started moving.

6) At the next snapshot, $\alpha = 35.7$ deg, the suction peaked has moved downstream, away from the leading edge and toward the half-chord; the lift coefficient is now 2.73.

7) At the next two snapshots, the suction peak moves downstream of the half-chord and decreases in strength. The lift coefficient drops rapidly back down to 2.04.

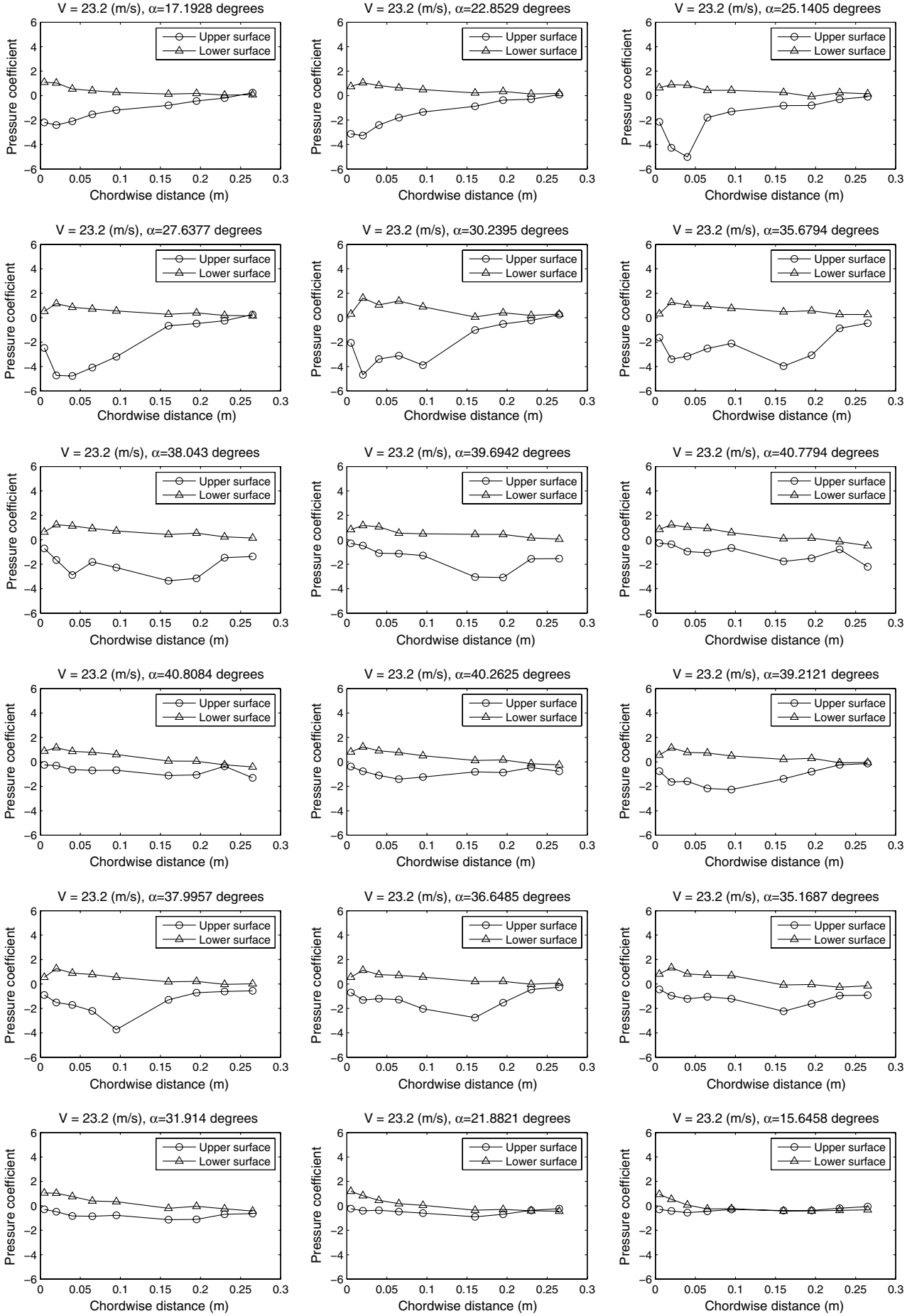

Fig. 28 Pressure distributions around airfoil during upper surface dynamic stall, $V = 23.2$ m/s.

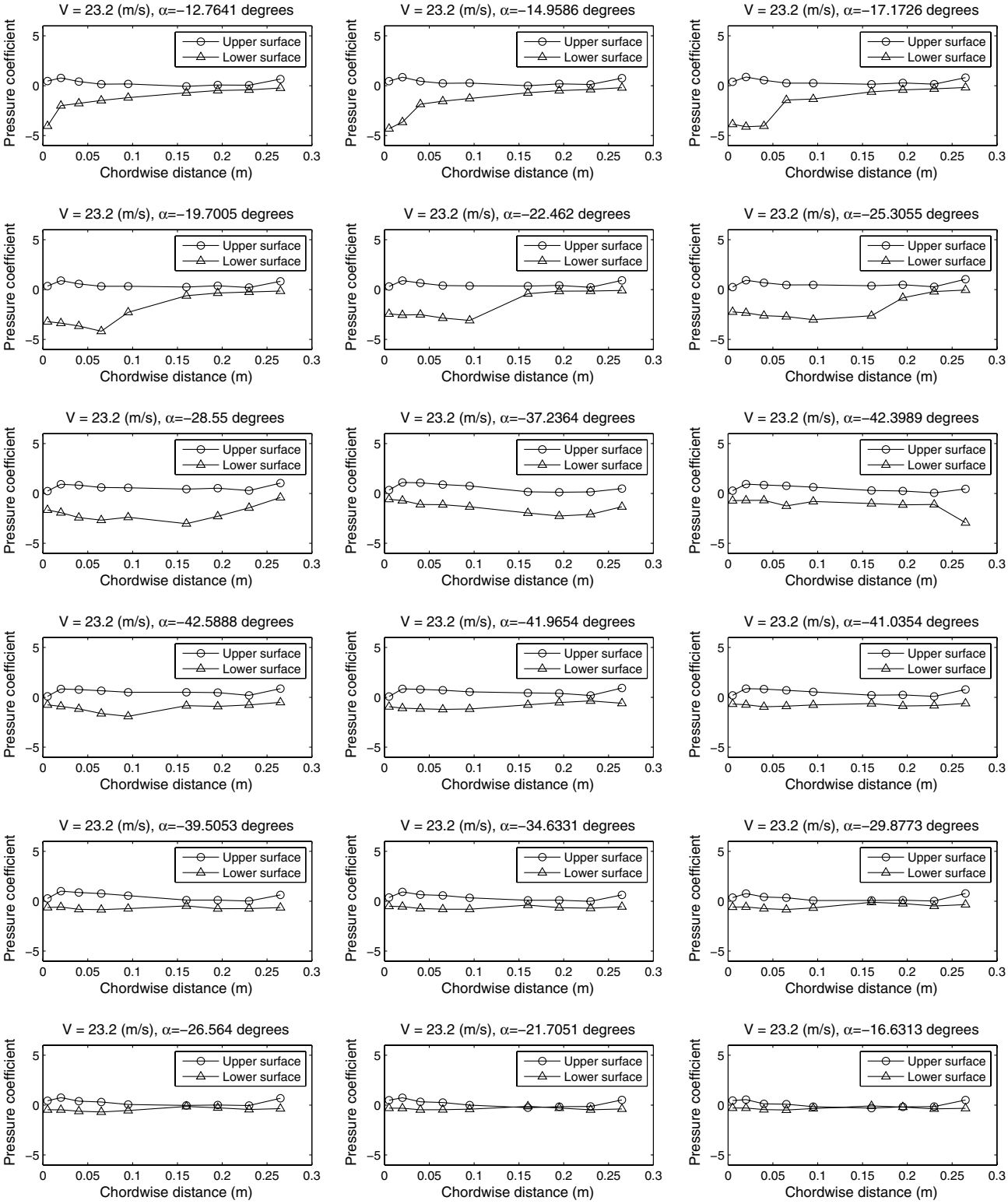

Fig. 29 Pressure distributions around airfoil during lower surface dynamic stall, $V = 23.2$ m/s.

8) At the maximum pitch displacement, $\alpha = 40.8$ deg, there is no more suction peak and the lift coefficient is back to the level of the first snapshot, 1.11.

9) As the pitch angle begins to decrease, the flow reattaches and the pressure difference between upper and lower surfaces increases again; the lift coefficient also increases to 1.47 at $\alpha = 39.2$ deg.

10) After further decreases in the pitch angle, a new suction peak appears, spreads, and moves downstream. The lift coefficient peaks at 1.75 when $\alpha = 36.6$ deg and then starts to decrease again. It must be mentioned that the appearance of this second suction peak coincides with an abrupt decrease in pitching moment coefficient around the pitch axis.

11) Between $\alpha = 38.0$ and $\alpha = 36.6$ deg, the pitching moment coefficient drops from 0.09 to −0.01.

12) At $\alpha = 31.9$ deg, the suction peak has completely disappeared and the lift coefficient has dropped to 0.88.

13) Finally, at $\alpha = 15.6$ deg, there is very little pressure difference between the upper and lower surfaces and the lift coefficient is 0.15.

The suction peaks observed in these snapshots are due to a vortex formed on the upper surface of the wing. The dynamic stall

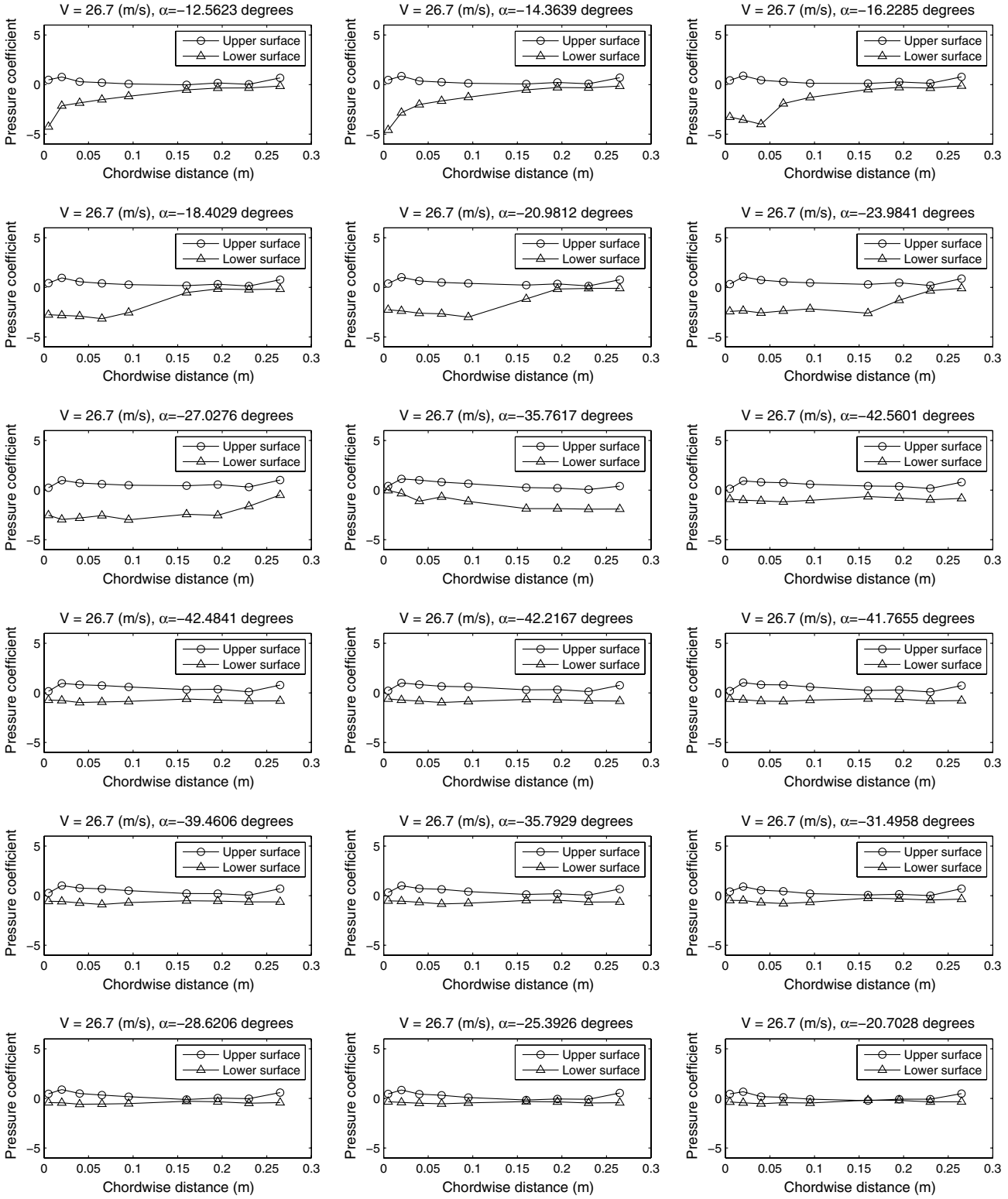

Fig. 30 Pressure distributions around airfoil during lower surface dynamic stall, $V = 26.7$ m/s.

phenomenon is occurring as a result of the creation of a dynamic stall vortex (DSV) and its propagation downstream. While the dynamic stall vortex is on the surface of the wing, it increases significantly the value of the lift coefficient. Once it clears the trailing edge, the lift coefficient drops abruptly, as does the pitching moment coefficient shortly afterward; this is the instance defined as dynamic stall. In this particular case, a second dynamic stall vortex is created and travels downstream, after the pitch angle starts to decrease again.

The dynamic stall vortex was first observed by McCroskey and Philippe [16], who carried out a set of experiments on a sinusoidally pitching airfoil. They used their observations to describe a complete dynamic stall mechanism, involving what later came to be known as the DSV. The mechanism behind the formation of the DSV became the subject of several subsequent works. Several authors believed that the vortex is formed as the result of the bursting of a laminar separation bubble at the leading edge (e.g., Fukushima and Dadone [27]).

The variation of the pressure distributions during a dynamic stall event on the lower surface of the wing at the same airspeed, $V = 23.2$, is shown in Fig. 29. This event is presented here to highlight the slight asymmetry of the stall flutter phenomenon observed during the experiments. The initial stages of the phenomenon are exactly the

same as in the upper surface stall case, although the maximum negative pitch angle is slightly higher at −42.6 deg. However, the major difference between the two events is the fact that, in the lower surface dynamic stall case, no secondary dynamic stall vortex is observed. The last three rows of Fig. 29 show that, as the pitch angle increases, the pressure distribution becomes thinner and thinner, until the lift coefficient is almost zero at $\alpha = -16.6$ deg. No further suction peaks are evident.

Figure 30 shows the variation of the pressure distribution with time during a lower surface dynamic stall even at $V = 26.7$ m/s. At this airspeed, the wing is undergoing the asymmetric LCO at negative pitch angles; dynamic stall occurs only on the lower surface, not on the upper surface. Despite this very important difference in the stall flutter phenomenon observed at this airspeed, the dynamic stall mechanism itself is quite similar to the one recorded at the lower airspeed of $V = 23.2$ and plotted in Fig. 29. The suction peak appears and develops slightly earlier (about 1.5 deg of pitch angle) but this fact is not particularly important; there are cycle-to-cycle variations at every airspeed. In every other respect, Figs. 29 and 30 are similar. This is quite an important conclusion because it means that the qualitative change of the stall flutter phenomenon from symmetric to asymmetric is not governed by a change in the dynamic stall mechanism.

Therefore, the only difference between the two airspeeds investigated here is that, in the asymmetric case, the wing will not stall on the upper surface. This fact reinforces the assertion that the asymmetric LCOs are caused by the static divergence phenomenon.

VI. Conclusions

The wind-tunnel tests described in this paper revealed a number of very interesting phenomena concerning a wing's stall flutter behavior and some of the parameters affecting it. The stall flutter observed was the result of the interaction between the dynamic stall, structural dynamics, and static divergence characteristics of the wind-tunnel model. Three types of response were observed, namely, decaying, symmetric LCO, and asymmetric LCO, and there were airspeed ranges in which some of these response types could coexist. The dynamic stall mechanism was observed in detail and was found to involve one or two major dynamic stall vortices that grow near the leading edge and then travel downstream. The present work showed that the mechanism is essentially the same in both the symmetric and asymmetric LCO cases. Furthermore, it seems that the secondary dynamic stall vortex is quite sensitive because it does not appear on the lower surface of the wing, probably due to the slight asymmetry in the wing shape.

The stall flutter phenomena can be described as a series of bifurcations, the first of which is a subcritical Hopf coupled with a fold, leading to symmetric LCOs. The second is a figure-eight homoclinic bifurcation caused by the interaction between static divergence and dynamic stall and leading to asymmetric LCOs. In the neighborhood of the subcritical Hopf, the wing can undergo either limit cycle or decaying oscillations. In the neighborhood of the pitchfork and homoclinic bifurcations, the wing can undergo either symmetric of asymmetric LCOs. It should be stressed that this bifurcation description can only be local in character as there is no mathematical model of the system and not all possible configurations of the wing were tested. For example, only cases where the equilibrium pitch angle is slightly positive or slightly negative were investigated. Large positive or negative values of the equilibrium pitch angle will be investigated in the future.

None of the periodic responses observed were strictly periodic; there were always some cycle-to-cycle differences. As a consequence, the bifurcation analysis presented here is based on the period-averaged forms of the observed LCOs. At airspeeds where more than one limit cycle coexisted, the cycle-to-cycle differences could force the wing to transit from one limit cycle to the other. At airspeeds where a limit cycle coexisted with a stable focal point, the cycle-to-cycle differences could force the wing to transit from the limit cycle to the focal point and vice versa.

The work presented here does not constitute a complete investigation of the stall flutter phenomenon. First of all, the Reynolds numbers tested were low compared to the Reynolds numbers involved in the stall flutter of retreating helicopter rotor blades or compressor blades. The Reynolds numbers investigated here are mostly compatible with the flow around wind turbines. Furthermore, the effect of several other parameters on the stall flutter behavior of the wing could be investigated, such as wing inertia, pitch and plunge stiffness, airfoil shape, 3-D flow effects, compressibility effects, and others.

The experimental results produced here could also be used to assist the simulation of this phenomenon. The data are available for comparison and/or calibration of computational fluid dynamics simulations. It should be mentioned, however, that the slight asymmetry of the wing shape was not exactly measured and this fact may hinder exact numerical comparisons.

Acknowledgments

The work presented in this paper was funded by the Engineering and Physical Sciences Research Council of the United Kingdom. The authors would like to thank Fengshu Gu, Ken Johnson, Michael Chapman, and all the people who used to work at the Goldstein Laboratory.

References

[1] Blevins, R. D., *Flow-Induced Vibration*, Van Nostrand Reinhold, New York, 1977.

[2] Halfman, R. L., Johnson, H. C., and Haley, S. M., "Evaluation of High-Angle-of-Attack Aerodynamic Derivative Data and Stall-Flutter Prediction Techniques," NACA TR TN 2533, 1951.

[3] Ericsson, L. E., and Reding, J. P., "Unsteady Airfoil Stall," NASA CR 66787, 1969.

[4] Ericsson, L. E., and Reding, J. P., "Analytic Prediction of Dynamic Stall Characteristics," AIAA Paper 72-682, June 1972.

[5] Ericsson, L. E., and Reding, J. P., "Stall-Flutter Analysis," *Journal of Aircraft*, Vol. 10, No. 1, 1973, pp. 5–13. doi:10.2514/3.60192

[6] Ericsson, L. E., and Reding, J. P., "Dynamic Stall at High Frequency and Large Amplitude," *Journal of Aircraft*, Vol. 17, No. 3, 1980, pp. 136–142. doi:10.2514/3.57884

[7] McCroskey, W. J., "The Phenomenon of Dynamic Stall," NASA TM 81264, 1981.

[8] Shih, C., Lurenco, L. M., and Krothapalli, A., "Investigation of Flow at Leading and Trailing Edges of Pitching-Up Airfoil," *AIAA Journal*, Vol. 33, No. 8, 1995, pp. 1369–1376. doi:10.2514/3.12560

[9] Wernert, P., Geissler, W., Raffel, M., and Kompenhans, J., "Experimental and Numerical Investigations of Dynamic Stall on a Pitching Airfoil," *AIAA Journal*, Vol. 34, No. 5, 1996, pp. 982–989. doi:10.2514/3.13177

[10] Lee, T., and Gerontakos, P., "Investigation of Flow over an Oscillating Airfoil," *Journal of Fluid Mechanics*, Vol. 512, 2004, pp. 313–341. doi:10.1017/S0022112004009851

[11] Victory, M., "Flutter at High Incidence," Aeronautical Research Com., Rept. and Memoranda No. 2048, 1943.

[12] Mendelson, A., "Effect of Aerodynamic Hysteresis on Critical Flutter Speed at Stall," NACA Research Memorandum No. E8B04, 1948.

[13] Ham, N. D., and Young, M. I., "Torsional Oscillation of Helicopter Blades Due to Stall," *Journal of Aircraft*, Vol. 3, No. 3, 1966, pp. 218–224. doi:10.2514/3.43728

[14] Rivera, J. A., Dansberry, B. E., Bennett, R. M., Durham, M. H., and Silva, W. A., "NACA0012 Benchmark Model Experimental Flutter Results with Unsteady Pressure Distributions," AIAA Paper 1992-2396, April 2004.

[15] Li, J., Dimitriadis, G., Gu, F., and Chen, Q., "Novel Instrumentation for the Measurement of the Unsteady Pressure Distribution Around a Wing Undergoing Stall Flutter Oscillations," Inst. of Acoustics Paper No. 3, Oct. 2007.

[16] McCroskey, W. J., and Philippe, J. J., "Dynamic Stall Experiments on Oscillating Airfoils," *AIAA Journal*, Vol. 14, No. 1, 1976, pp. 57–63. doi:10.2514/3.61332

[17] Tsang, K., So, R., Leung, R., and Wang, X., "Dynamic Stall Behavior

from Unsteady Force Measurements," *Journal of Fluids and Structures*, Vol. 24, No. 1, 2008, pp. 129–150. doi:10.1016/j.jfluidstructs.2007.06.007

[18] Kuznetsov, Y. A., *Elements of Applied Bifurcation Theory*, Springer–Verlag, New York, 1998.

[19] Holmes, P., "Bifurcations to Divergence and Flutter in Flow-Induced Oscillations: An Infinite Dimensional Analysis," *Automatica*, Vol. 14, No. 4, 1978, pp. 367–384. doi:10.1016/0005-1098(78)90036-5

[20] Chen, Y., and Leung, A. Y. T., *Bifurcation and Chaos in Engineering*, Springer, New York, 1998.

[21] Allgower, E. L., and Georg, K., *Numerical Continuation Methods: An Introduction*, Springer–Verlag, New York, 1990.

[22] Jordan, D. W., and Smith, P., *Nonlinear Ordinary Differential Equations: An Introduction to Dynamical Systems*, Oxford Applied and Engineering Mathematics, 3rd ed., Oxford Univ. Press, Oxford, England, U.K., 1999.

[23] Guckenheimer, J., and Holmes, P., *Nonlinear Oscillations, Dynamical Systems, and Bifurcations of Vector Fields*, Vol. 42, Applied Mathematical Sciences, Springer, New York, 1983.

[24] Strogatz, S. H., *Nonlinear Dynamics and Chaos: With Applications to Physics, Biology, Chemistry, and Engineering*, Perseus Books, Cambridge, MA, 1994.

[25] Verhulst, F., *Nonlinear Differential Equations and Dynamical Systems*, 2nd ed., Springer–Verlag, London, 1996.

[26] Juel, A., Darbyshire, A. G., and Mullin, T., "The Effect of Noise on Pitchfork and Hopf Bifurcations," *Proceedings of the Royal Society of London A*, Vol. 453, No. 1967, 1997, pp. 2627–2647. doi:10.1098/rspa.1997.0140

[27] Fukushima, T., and Dadone, L. U., "Comparison of Dynamic Stall Phenomena for Pitching and Vertical Translation Motions," NASA CR 2793, 1977.

P. Beran
Associate Editor